1   *Article*   *October 19, 2018*

2

3

4   **MYC Functions as a Switch for Natural Killer Cell-Mediated Immune Surveillance of**

5   **Lymphoid Malignancies**

6   Srividya Swaminathan[1], Line D. Heftdal[1], Daniel F. Liefwalker[1], Renumathy Dhanasekaran[2],

7   Anja Deutzmann[1], Crista Horton[1], Adriane Mosley[1], Mariola Liebersbach[1], Holden T. Maecker[3],

8   and *Dean W. Felsher[1]

9

10   [1]*Division of Oncology, Departments of Medicine and Pathology, Stanford University, Stanford,*
11   *CA, USA,* [2]*Division of Gastroenterology and Hepatology, Stanford University, Stanford, CA,*
12   *USA,* [3]*The Human Immune Monitoring Center (HIMC), Institute for Immunity, Transplantation*
13   *and Infection, Stanford University School of Medicine,*
14   *Stanford, California, USA.*
15

16   **Abbreviations:**
17   CyTOF, Cytometry Time of Flight; BL, Burkitt's Lymphoma; ALL, Acute Lymphoblastic
18   Leukemia; DLBCL, Diffuse Large B Cell Lymphoma; NK Cell, Natural Killer Cell; STAT1/2,
19   Signal Transducer and Activator of Transcription 1/2; IFN, Interferon; DC, Dendritic Cell;
20   MYC, v-myc avian myelocytomatosis viral oncogene homolog; PRECOG, Prediction of Clinical
21   Outcomes from Genomic Profiles; BLI, Bioluminescence Imaging; TSS, Transcriptional Start
22   Site; HTLV, Human T-lymphotropic Virus; hMYC, human MYC.
23

24   ***For correspondence:**
25   Dean W. Felsher, MD PhD
26   Division of Medical Oncology
27   Departments of Medicine and Pathology
28   Stanford University, Stanford, CA
29   E-mail: dfelsher@stanford.edu
30
31

32   **Running Title:**
33   Oncogenic MYC blocks NK cell-mediated immune surveillance

1

34 **Abstract**

35 The MYC oncogene drives T and B lymphoid malignancies, including Burkitt's lymphoma (BL)

36 and Acute Lymphoblastic Leukemia (ALL). Using CyTOF, we demonstrate a systemic reduction

37 in natural killer (NK) cell-mediated surveillance in $SR\alpha\text{-}tTA/Tet\text{-}O\text{-}MYC^{ON}$ mice bearing MYC-

38 driven T-lymphomas, due to an arrest in NK cell maturation. Inactivation of lymphoma-intrinsic

39 MYC releases the brakes on NK maturation restoring NK homeostasis. Lymphoma-intrinsic

40 MYC arrests NK maturation by transcriptionally repressing STAT1/2 and secretion of Type I

41 Interferons (IFNs). Treating T-lymphoma-bearing mice with Type I IFN improves survival by

42 rescuing NK cell maturation. In MYC-driven BL patients, low expression of both STAT1 and

43 STAT2 correlates significantly with the absence of activated NK cells and predicts unfavorable

44 clinical outcomes. Adoptive transfer of mature NK cells is sufficient to delay both T-lymphoma

45 growth and recurrence post MYC inactivation. Our studies thus provide a rationale for

46 developing NK cell-based therapies to effectively treat MYC-driven lymphomas in the future.

47   Oncogene addiction is the phenomenon where a cancer becomes causally dependent on a single

48   'driver' oncogene for the maintenance of its proliferation and survival [1,2]. Inhibition of the driver

49   oncogene forms the basis of oncogene targeted therapy [1–3]. Hence, a potential Achilles' heel of

50   human malignancies lies in their addiction to oncogenes such as *MYC*, *RAS* and *BCR-ABL1* [4,5].

51   Targeted therapy has been successful against BCR-ABL1 (Philadelphia/Ph[+])-induced leukemia

52   [6,7], while therapies that successfully target MYC or RAS remain to be developed.

53   In order to develop targeted therapies for MYC-driven cancers, it is vital to understand

54   whether MYC regulates both cell autonomous and non-autonomous processes, including host

55   immunity. Oncogene addiction was previously assumed to be cell autonomous and immune-

56   independent [8]. Many recent studies illustrate that MYC and other oncogenes alone or

57   cooperatively may regulate the tumor microenvironment and host immune responses in multiple

58   tumor types [9–16]. In particular, two reports highlighted that oncogenes may cooperate to more

59   globally regulate the host immune system [12,16].

60   We have used a particularly tractable approach for studying the role of the host immune

61   system during MYC-driven tumorigenesis through tetracycline (tet)-system regulated transgenic

62   mouse models of cancer. Our inducible mouse models enable us to study how MYC inactivation

63   elicits tumor regression through both cancer-intrinsic and cancer-extrinsic host immune-

64   dependent mechanisms [11,13]. CD4^{+} T cells appear to be essential for the sustained regression of

65   cancers upon MYC inactivation [11,13]. However, the changes in immune landscape during primary

66   MYC-induced tumorigenesis in these models remain to be delineated.

67   Our goal was to delineate the global immunological changes resulting from primary overt

68   MYC-driven lymphomagenesis, to identify anti-tumor immune subsets that can be developed as

69   therapies to treat MYC-driven lymphomas. We hypothesized that oncogenic MYC directly

3

70   perturbs the global immune composition at sites of primary lymphomagenesis to evade immune

71   surveillance. Hence, using mass cytometry (CyTOF), we examined specific changes in the host

72   immune composition both upon MYC activation as well as after subsequent MYC inactivation *in*

73   *situ* in *SRα-tTA/tet-O-MYC* mice predisposed to developing autochthonous MYC-driven T cell

74   lymphoblastic lymphoma [1].

75   We observed that MYC markedly suppresses maturation and production of natural killer

76   (NK) cells in the lymphoma microenvironment. Furthermore, we found that NK cells play a key

77   anti-tumorigenic role by delaying the growth and recurrence of MYC-driven T cell lymphomas,

78   and are hence, suppressed by MYC during overt lymphomagenesis. We found a direct signaling

79   mechanism by which lymphoma-intrinsic MYC suppresses NK cell-mediated immune

80   surveillance. Our results provide a rationale for developing NK cell-based therapies that can be

81   combined with MYC inhibitors to treat MYC-driven lymphomas.

82 **Results**

83 ***MYC-driven lymphomas exhibit disrupted splenic architectures***

84 First, we evaluated the gross changes in lymphoid organs resulting from primary overt

85 MYC-driven T cell lymphomagenesis in *SRα-tTA/tet-O-MYC* mice [1]. Of note, SRα (a

86 component of human T-lymphotropic virus; HTLV) restricts the overexpression of the human

87 MYC (hMYC) transgene to the T cell lineage in *SRα-tTA/tet-O-MYC* mice, thus giving rise to

88 systemically disseminated T cell lymphomas [1]. Lymphoma-bearing mice displayed splenic

89 germinal center disruption while inhibition of MYC partially rescued the germinal center

90 architecture of the spleen (**Supplementary Figure 1**). These findings suggested that MYC

91 overexpression in T cell lymphoma might remodel the splenic immune architecture.

92

93 ***Oncogenic MYC perturbs the relative proportions of splenic immune subsets***

94 Inducible regulation of the hMYC transgene specifically in malignant T-lymphocytes

95 enables us to elucidate how lymphoma-intrinsic MYC impacts normal immune cells during

96 primary lymphomagenesis. Our goal was to identify anti-tumor immune subsets that can be

97 developed as therapies against MYC-driven lymphomas. Hence, using CyTOF [17], we delineated

98 the global changes in the immune compositions of lymphoid organs during primary MYC-driven

99 lymphomagenesis in *SRα-tTA/tet-O-MYC* mice.

100 Spleen was chosen for CyTOF experiments for two reasons. First, the spleen contains a

101 diverse immune population including T and B lymphocytes, NK cells, dendritic cells (DCs), and

102 myeloid cells that enable us to study interactions between lymphoma cells and their immune

103 microenvironment *in situ*. Second, the lack of immature pre-T cells in the spleen allows us to

104 visualize the infiltration of immature T cell lymphoblasts in MYC^{ON} mice and distinguish them

5

105   from healthy and MYC^{OFF} mice. Primary splenic samples derived from overt lymphoma-bearing

106   *SRα-tTA/tet-O-MYC* mice before (MYC^{ON}, n = 9) and after (MYC^{OFF}, 96h, n = 10) MYC

107   inactivation were examined for immune subsets; and compared to age-matched normal wildtype

108   spleens (Normal, n = 11).

109   Normal spleens contain mature single positive (SP) helper CD4^{+} T (CD3^{+} CD4^{+} CD8^{-})

110   and cytotoxic CD8^{+} T (CD3^{+} CD4^{-} CD8^{+}) cells, and are nearly devoid of immature double

111   positive (DP, CD3^{+} CD4^{+} CD8^{+}) and immature double negative (DN, CD3^{+} CD4^{-} CD8^{-}) subsets.

112   Consistent with the phenotype of a T cell lymphoma, the distribution of T cell subsets was

113   altered in the MYC^{ON} cohort with an increase in the percentages of immature CD4^{+} CD8^{+} DP

114   CD3^{+} T-cell leukemic blasts as compared to normal mice (**Figures 1a-c, Supplementary**

115   **Figures 2a-b**). MYC inactivation (MYC^{OFF}) resulted in elimination of most DP T cell blasts and

116   restored the distribution of splenic T cell subsets to normal levels, demonstrating MYC-

117   addiction, as previously described [1] (**Figures 1a-c, Supplementary Figures 2a-b**). Malignant

118   CD3^{+} T-lymphocytes in MYC^{ON} mice are TCRαβ^{+}, thus leading to a reduction in the

119   percentages of TCRγδ^{+} T cells (**Supplementary Figures 2c-d**).

120   We next examined the other non-malignant immune compartments that do not express

121   the T cell specific hMYC transgene in *SRα-tTA/tet-O-MYC* mice before (MYC^{ON}) and after

122   (MYC^{OFF}) MYC inactivation, and compared these to normal mice. Amongst these normal

123   subsets, percentages of NK (CD3^{-} NKp46^{+}, **Figure 1d, Supplementary Figures 2e-f**), and B

124   cell (CD19^{+}, **Figure 1e, Supplementary Figures 3a-b**) subsets were significantly lowered in

125   MYC^{ON} overt lymphoma-bearing mice. Yet, NK (**Figure 1d, Supplementary Figures 2e-f**), and

126   B cell (**Figure 1e, Supplementary Figures 3a-b**) percentages were restored close to normal

127   levels in MYC^{OFF} mice. The relative proportions of other immune compartments including

128   myeloid compartments such as dendritic cells (DCs) and neutrophils were unaltered by the

129   activation of oncogenic MYC (**Supplementary Figures 3c-f**).

130

131   ***Immune composition of MYC-driven lymphomas is altered independently of splenomegaly***

132   Lymphomagenesis is often associated with splenomegaly and increased splenic

133   cellularity. Therefore, we had to rule out the possibility that the apparent reduction in immune

134   subsets such as, NK and B cells was because they were being passively outnumbered by

135   invading MYC-driven malignant lymphocytes. To address this, we measured the absolute cell

136   numbers of the immune subsets in the splenic samples evaluated by CyTOF. Notably, we

137   observed a statistically significant increase in the cellularity of lymphoma spleens (**Figure 1f**).

138   As expected, the absolute cell counts of $CD3^+$ pan T (**Supplementary Figure 4a**), $TCR\alpha\beta^+$

139    $CD3^+$ T (**Supplementary Figure 4b**) and immature $CD4^+$ $CD8^+$ double positive (DP) $CD3^+$

140   leukemic T cells (**Figure 1g**) were increased in MYC^{ON} mice when compared to normal and

141   MYC^{OFF} mice. Characteristic with the properties of a lymphoma, abundant multiplication of the

142    $TCR\alpha\beta^+$ $CD3^+$ T cell lymphoblasts was accompanied by a significant reduction in numbers of

143    $CD3^+$ $TCR\gamma\delta^+$ $\gamma\delta$ T cells in MYC^{ON} mice (**Supplementary Figure 4c**).

144   Oncogenic MYC significantly lowered absolute cell numbers of $CD3^-$ $NKp46^+$ NK cells,

145   whereas MYC inhibition significantly reversed this effect (**Figure 1h**). Absolute numbers of B

146   cells were unaltered in MYC-driven lymphomas as compared to healthy controls and MYC^{OFF}

147   mice (**Figure 1i**), although B cell percentages had been significantly reduced in lymphoma-

148   bearing mice (**Figure 1e, Supplementary Figures 3a-b**). MYC-driven lymphomagenesis

149   significantly increased numbers of pan $CD11c^+$ DCs and neutrophils (**Supplementary Figures**

150   **4d-e**). The increase in numbers of DCs and neutrophils during MYC-driven lymphomagenesis

151   corroborated the previously well-characterized pro-tumorigenic functions of these subsets in

152   lymphomas [18–20].

153

NK cells represent a key anti-tumorigenic immune compartment suppressed during MYC-driven lymphomagenesis

156   Our goal was to identify anti-tumor immune subsets that can be developed as therapies

157   against MYC-driven lymphomas. Amongst the anti-tumorigenic immune subsets (NK and B

158   cells) altered during MYC-driven lymphomagenesis, NK cells particularly stood out for the

159   following reasons: First, NK cells were the sole subset significantly altered both in absolute cell

160   numbers (**Figure 1h**) and percentages (**Figure 1d, Supplementary Figures 2e-f**). Second, MYC

161   inactivation restores NK cell compositions suggesting that oncogenic MYC may directly regulate

162   this immune subset (**Figures 1d, h**). Third, we observed a significant suppression of maturation

163   and cytotoxicity marker NKp46 [21] on the surface of residual NK cells in MYC^{ON} spleens when

164   compared to normal and MYC^{OFF} spleens (**Figure 1j**). Fourth, NK cells are attractive as a

165   potential cell-based immunotherapy against MYC-driven lymphomas. Hence, we focused

166   specifically on how oncogenic MYC alters the NK subset during lymphomagenesis.

167   We confirmed our CyTOF results which show an inverse correlation between the activity

168   of MYC and NK cell presence, by measuring NK cell compositions before and after MYC

169   inactivation by conventional flow cytometry (**Supplementary Figure 5**). Next, using

170   CIBERSORT [22], a computational method for determining immune compositions from bulk gene

171   expression data, we estimated changes in NK composition in CyTOF-matched spleens from

172   normal (n = 3), SRα-tTA MYC^{ON} (lymphoma, n = 3) and SRα-tTA MYC^{OFF} (regressed

173   lymphoma, n = 3) mice. Concordant with CyTOF results, CIBERSORT also demonstrates a

8

174   reduction in the relative proportion of the NK cells in MYC^{ON} mice when compared to normal

175   and MYC^{OFF} mice (**Supplementary Figure 6**). Hence, using three different platforms (CyTOF,

176   flow cytometry, and CIBERSORT), we were able to robustly demonstrate that oncogenic MYC

177   causally and reversibly reduces splenic NK cell-mediated immune surveillance during

178   lymphomagenesis (**Figure 1k**).

179

180   ***NK cell suppression during MYC-driven lymphomagenesis is systemic in nature***

181   We examined whether the phenomenon of NK cell suppression occurs in other lymphoid

182   organs infiltrated by malignant T cell lymphoblasts, including blood (**Figures 2a-e**) and bone

183   marrow (**Supplementary Figure 7**). Circulating NK cell percentages (**Figures 2b-c**), numbers

184   per μl of blood (**Figure 2d**), and maturation (NKp46 MFI, **Figure 2e**) were significantly reduced

185   in overt lymphoma mice (MYC^{ON}, n = 6), as compared to normal (n = 6) and MYC-inactivated

186   (MYC^{OFF}, n = 6) mice.

187   Next, we investigated whether MYC-driven T cell lymphomagenesis leads to NK cell

188   suppression in the bone marrow. T cell lymphoma in our model manifests with significant bone

189   marrow involvement (**Supplementary Figures 7a-d**). CD3$^-$ NKp46$^+$ mature NK cells were

190   significantly suppressed in bone marrow of lymphoma-bearing mice (MYC^{ON}, n = 7), as

191   compared to normal (n = 9) and MYC-inactivated (MYC^{OFF}, n = 7) mice (**Supplementary**

192   **Figures 7e-f**). NK cell numbers in the bone marrow were significantly restored following MYC

193   inactivation (**Supplementary Figures 7e**).

194

195   ***NK cell suppression during lymphomagenesis is MYC-dependent***

196   We next demonstrated the dependency of NK suppression on MYC status, by comparing

197   percentages and surface NKp46 expression of splenic (**Figures 2f-h**) and circulating (**Figures 2i-**

198   **k**) NK cells in MYC^{OFF} mice (with residual blasts) alongside lymphoma-bearing mice (MYC^{ON})

199   with similar blast percentages. The presence of residual lymphoblasts in MYC^{OFF} mice may be

200   attributed to (**1**) initial high disease burden before inactivating MYC, or (**2**) partial differentiation

201   of lymphoblasts after MYC inactivation [23]. We observed that MYC inactivation increases NK

202   cell percentages (**Figures 2g, j**) and the expression of NK cell maturation and cytotoxicity

203   marker NKp46 (MFI surface NKp46, **Figures 2h, k**) even in the presence of residual

204   lymphoblasts (**Figures 2f, i**). Hence, we infer that NK cell suppression is MYC-dependent, and

205   does not occur simply due to the creation of niche space vacated by the clearance of lymphoma

206   cells following MYC inactivation.

207

208   ***Maturation of NK cells is arrested during MYC-driven lymphomagenesis***

209   We investigated whether reduction in mature CD3$^-$ NKp46$^+$ NK cells during MYC-

210   induced lymphomagenesis occurs because of increased cell death. Surprisingly, we observed

211   reduced death of NK cells at sites of lymphomagenesis in lymphoma-bearing MYC^{ON} mice, in

212   comparison to normal and MYC^{OFF} cohorts (**Supplementary Figure 8**). Hence, suppression of

213   NK subset during lymphomagenesis is not caused by increased apoptosis of NK cells induced by

214   lymphomagenic MYC.

215   The disappearance of NK cells from the bone marrow of MYC^{ON} mice (**Supplementary**

216   **Figure 7**) suggested that MYC-driven lymphomagenesis might abrogate the replenishment of

217   mature CD3$^-$NKp46$^+$ NK cells in the periphery possibly by blocking early NK cell development

218   [24–27]. We tested this possibility by comparing the absolute counts of NK cell precursors (NKP,

10

219   CD122$^+$ NKp46$^-$, **Figure 3a**), and the more differentiated CD122$^+$ NKp46$^+$ iNK (immature NK,

220   **Figure 3b**) cells in bone marrow from normal (n = 8), SRα-tTA MYC^{ON} (lymphoma, n = 8), and

221   SRα-tTA MYC^{OFF} (regressed lymphoma, n = 8) mice. While we observed no significant changes

222   in the numbers of NKP across the three groups, the numbers of iNK cells were significantly

223   reduced in MYC^{ON} bone marrow, in comparison to MYC^{OFF} and normal bone marrows (**Figures**

224   **3a-b**). Consistent with these observations, the ratio of counts of NKP vs iNK were significantly

225   enhanced in individual MYC^{ON} mice in comparison to healthy and MYC^{OFF} mice (**Figure 3c**).

226   We infer that oncogenic MYC blocks the expression of NKp46 and hence, the transition

227   from NKP to iNK stage of NK cell maturation in the bone marrow [24,25]. The spleens of MYC^{ON}

228   mice exhibited no changes in the CD122$^+$ NKp46$^-$ NKP, and a significant reduction in the more

229   differentiated CD122$^+$ NKp46$^+$ iNK fraction (**Figures 3e-h**), concordant with the changes

230   observed in their corresponding bone marrows (**Figures 3a-d**). Hence, NK cells are systemically

231   suppressed during MYC-induced lymphomagenesis because of arrested NK cell maturation in

232   the bone marrow that translates to the periphery (**Figure 3i**).

233

234   ***Suppression of Type I IFN signature during primary MYC-driven lymphomagenesis may***

235   ***block NK cell-mediated immune surveillance***

236   We next investigated the molecular mechanisms by which oncogenic MYC may suppress

237   NK cell-mediated immune surveillance during primary T and B cell lymphomagenesis. To this

238   end, we analyzed the global transcriptomic profiles of bulk splenic cells from normal (n = 3),

239   SRα-tTA MYC^{ON} (lymphoma, n = 3) and SRα-tTA MYC^{OFF} (regressed lymphoma, n = 3) mice

240   (GSE106078). We observed that the expression profiles of MYC^{OFF} spleens clustered closely

241   with normal spleens, thus confirming that transcriptional changes induced by MYC were largely

11

242   reversible upon its inactivation (**Figure 4a**). Gene set enrichment analyses (GSEA) revealed that

243   the JAKs (Janus Kinases) – STAT1/2 (Signal Transducer and Activator of Transcription 1/2) –

244   Type I IFN (Interferon) pathway was significantly suppressed in MYC^{ON} mice when compared

245   to normal and MYC^{OFF} mice (**Figures 4b-d**, **Supplementary Figure 9**). Of note, the activation

246   of STAT1/2 post MYC inactivation resembles an anti-viral immune response that is associated

247   with production of Type I IFNs and subsequent activation of NK cell-mediated immune

248   surveillance [28].

249   STAT1/2-Type I IFN signaling has been previously demonstrated to be required for

250   maturation and expansion of NK cells before the expression of NKp46 at the iNK stage [29–35]. Of

251   note, mice deficient in Type I IFN receptor (*IFNαR$^{-/-}$*) show significantly lower numbers of NK

252   cells in spleen when compared to normal mice [29,35]; a phenomenon we observe during MYC-

253   driven lymphomagenesis (**Figure 1h**). Concordant with our results of NK cell suppression as a

254   result of MYC-driven lymphomagenesis (**Figures 1-2**), we observed transcriptional repression of

255   a number of Type I IFN regulated genes that are specific to NK-mediated immune surveillance

256   in MYC^{ON} mice, when compared to normal and MYC^{OFF} mice (**Figure 4e**). These findings

257   suggested the possibility of existence of a link between Type I IFN signature and the observed

258   splenic NK cell profiles of each group.

259   Next, we compared transcript levels of STAT1, STAT2 and other important Type I IFN

260   signaling components in normal B cells (MYC^{LOW}, n = 4), pre-lymphoma B cells from Eμ-MYC

261   mice (MYC^{HIGH}, n = 4), and overt B cell lymphoma from Eμ-MYC mice (MYC^{HIGH}, n = 2),

262   which is an independent mouse model of MYC-driven B cell lymphoma (GSE51011, [36]).

263   Sequential increase in MYC during stepwise B cell transformation is accompanied by

264   transcriptional suppression of STAT1/2-Type I IFN signature (**Supplementary Figure 10**).

12

265   Hence, suppression of STAT1/2-Type I IFN signaling is a signature of both T cell and B cell

266   MYC-driven lymphomagenesis.

267

268   ***MYC-mediated suppression of NK cells can reversed by Type I IFN treatment***

269   We investigated whether short-term (3 days) administration of Type I IFN to SRα-tTA

270   MYC^{ON} mice bearing overt T cell lymphoma can rescue MYC-mediated NK cell suppression,

271   and increase infiltration of NK cells into spleens (**Figures 4f-j**). The percentages and numbers of

272   CD3$^-$ NKp46$^+$ NK cells were significantly increased in IFNα-treated mice (n = 5) when

273   compared to corresponding litter-matched lymphoma mice treated with vehicle (PBS, n = 5)

274   (**Figures 4f, 4j**). Of note, total numbers and percentages of WBC, CD3$^+$ T cells and DP

275   immature T cells remain unaltered between the control and IFNα-treated groups (**Figures 4g-i**),

276   thus highlighting that Type I IFNs specifically regulate NK cell homeostasis and do not exert any

277   direct anti-proliferative effects on tumor cells. Long-term administration of Type I IFNs to SRα-

278   tTA MYC^{ON} mice bearing overt T cell lymphomas (n = 8) improves overall survival (OS) in

279   comparison to vehicle (PBS)-treated (n = 8) lymphoma-bearing mice (**Figure 4k**). Hence, we

280   conclude that MYC-driven lymphomagenesis may subvert normal immunological processes of

281   NK cell homeostasis by suppressing STAT1/2 signaling cascade and Type I IFN production.

282

283   ***Lymphoma-intrinsic MYC suppresses Type I IFN production by tumor cells***

284   We hypothesized that signals blocking NK cell maturation arise from MYC-driven

285   lymphoma cells for two reasons. First, we observed that suppression of NK cells is dependent on

286   the MYC status of T cell lymphoblasts (**Figures 2f-k**). Second, we showed that MYC-

287   overexpressing lymphoblasts display suppression of STAT1/2-Type I IFN signaling during

13

288   primary lymphomagenesis (**Supplementary Figure 10**). Hence, as the next step, we investigated

289   whether modulation of oncogenic MYC *in vitro* in MYC-driven B and T lymphoma cell lines

290   differentially regulates STAT1/2-Type I IFN signaling.

291   Since BL is a classic human MYC-associated lymphoid cancer, we measured signaling

292   changes by Phospho-CyTOF before (MYC^{ON}) and after (MYC^{OFF}) MYC inactivation in an

293   EBV-transformed human B cell line that expresses MYC regulated by the Tet System (P493-6),

294   and mimics BL [37] (**Supplementary Figure 11**). We confirmed that MYC is inducibly expressed

295   in P493-6 cells (**Figure 5a**). Amongst the key immune regulatory cytokine signaling pathways

296   that operate through the JAKs and STATs, MYC suppressed the activation of STAT1 in P493-6

297   cells (**Figures 5b-c, Supplementary Figure 11**). MYC inactivation increased STAT1

298   phosphorylation and activity (**Figures 5b-c**), STAT1 transcription (**Figure 5d, Supplementary**

299   **Figure 12a**) and STAT1 protein production (**Figure 5c**). Transcription of STAT2, the binding

300   partner of STAT1, was also induced post MYC inactivation in P493-6 cells (**Figure 5d,**

301   **Supplementary Figure 12b**).   Indeed, the transcript level of Type I IFN, IFNα2 was

302   significantly elevated after MYC inactivation in P493-6 cells (MYC^{OFF}, **Figure 5e**).

303   Comprehensive cytokine profiling of the P493-6 cells pre- and post- MYC inactivation

304   (**Supplementary Figure 13**) demonstrated that the secretion of IFNα is significantly upregulated

305   in the MYC^{OFF} cells in comparison to the MYC$^{ON/HIGH}$ population (**Figure 5f**).

306   Tumor-intrinsic signaling changes post MYC inactivation in our T cell lymphoma line

307   derived from *SRα-tTA/tet-O-MYC* mice (**Supplementary Figure 14**) mirrored those observed in

308   the human BL-like model with MYC inactivation leading to activation of STAT1/2-Type I IFN

309   signaling (**Supplementary Figure 15**). Our findings suggested that lymphoma-intrinsic MYC

14

310   represses STAT1/2-Type I IFN signaling; thereby blocking the maturation of NK cells in the

311   tumor microenvironment, and NK cell-mediated immune surveillance.

312

313   ***MYC transcriptionally represses the activation of STAT1/2-Type I IFN signaling***

314   We tested the possibility of MYC transcriptionally repressing the STAT1/2-Type I IFN

315   signaling cascade. Although widely known as a transactivator, MYC can inhibit the transcription

316   of genes by sequestering transactivators such as MIZ1 and Sp1/Sp3 [38–40], and binding to Initiator

317   (Inr) elements in gene promoters. For example, MYC inactivation releases MYC-MAX

318   heterodimers from the binding sites of tumor suppressor genes such as *Cdkn2b* and *Cdkn1b*,

319   thereby promoting MIZ1-mediated transcriptional activation of these genes [38–40].

320   Concordant with a previous study where MYC was shown to transcriptionally repress

321   STAT1 [41], we found that MYC binds the STAT1 promoter in P493-6 human BL and mouse

322   MYC-driven T cell lymphoma (**Supplementary Figure 16**). In order to delineate the molecular

323   mechanism behind MYC-mediated transcriptional repression of Type I IFN signaling, we

324   compared levels of STAT1, STAT2, and IFNα2 in MYC-driven lymphoma cell lines

325   overexpressing MYC, or a MYC mutant that fails to sequester MIZ1 (MYC V394D), or the

326   corresponding empty vector (EV). While MYC overexpression in P493-6 cells effectively

327   repressed the production of STAT1/2 (**Figures 5g-j**) and IFNα2 (**Figure 5k**), the MYCV394D

328   mutant significantly rescued the activation of STAT1/2-Type I IFN signaling, both before and

329   after inactivation of tetracycline-controlled MYC (Tet-MYC). Our results show that MYC

330   transcriptionally represses STAT1/2-Type I IFN signaling partially by sequestering

331   transactivators such as MIZ1. In MYC-driven T-ALL cells, we observe that MYC-mediated

332   suppression of the Type I IFN signaling cascade is independent of MIZ1 (**Supplementary**

15

333   **Figure 17**), suggesting the possible involvement of other MYC binding partners such as SP1/3

334   [40].

335

MYC^High human lymphomas exhibit suppression of STAT1/2 and NK cell-mediated immune

surveillance

338   We examined MYC-driven human lymphoma patients for evidence of repression of

339   STAT1/2 signaling and NK cell-mediated immune surveillance. First, we analyzed human

340   lymphomas that often exhibit MYC hyperactivation, such as Burkitt's Lymphoma (BL) and

341   Diffuse Large B Cell Lymphoma (DLBCL, GSE4475 [42]). We observed that STAT1 and STAT2

342   levels inversely correlate with MYC levels in BL (n = 34, blue) and DLBCL (n = 187, orange)

343   patients (**Figures 6a-b**). Of note, the BL subset driven directly by MYC translocations [43]

344   displays the highest MYC levels in combination with the lowest levels of STAT1 and STAT2

345   (**Figures 6a-b**). Hence, we concluded that natural addiction to MYC in the BL subgroup might

346   lead to the suppression of STAT1/2-Type I IFN signaling.

347   Next, we analyzed whether separation of BL patients into four groups based on their

348   median expressions of both STAT1 and STAT2 can predict clinical prognosis. We observed that

349   patients with the lowest levels of both STAT1 and STAT2 had the most unfavorable clinical

350   outcome (**Figure 6c**). We observed that majority (85%, 6/7) of BL patients (n = 34) with lowest

351   levels of both STAT1 and STAT2 have no activated NK cells (**Figure 6d**), as estimated by

352   CIBERSORT. We found that higher levels of activated NK cells were associated with a

353   significantly favorable clinical outcome and prolonged BL patient survival (**Figure 6e**). Hence,

354   we conclude that low expression of both STAT1 and STAT2 ($STAT1_{Low}$ $STAT2_{Low}$) coincides

16

355   both with maximum NK cell suppression (No activated NK, **Figure 6d**) and poor overall

356   survival in BL patients (**Figures 6c, 6e**).

357   Finally, using CIBERSORT on bulk expression data, we compared the estimated

358   fractions of NK cells in mononuclear cells isolated from blood of oncogene-addicted human T-

359   lymphoma patients (n = 48, GSE62156) [44,45] and normal healthy individuals (n = 20) [22]. Of note,

360   MYC levels are significantly higher in T cell lymphoma patients as compared to healthy

361   individuals (**Figure 6f**) because of chromosomal translocations that can potentially activate

362   MYC [44–50]. We observed a significant suppression of STAT1 and STAT2 levels (**Figures 6g-h**),

363   and a reduction in total and activated NK cell subsets in human T cell lymphoma patients in

364   comparison to their normal counterparts (**Figures 6i-l**). Collectively, our findings suggest a

365   common paradigm of NK cell suppression in both human and mouse MYC-driven lymphomas,

366   that occurs in part due to the direct repression of the STAT1/2-Type I IFN signaling cascade by

367   the MYC oncogene.

368

369   ***NK cells may represent a potential cell-based therapeutic against MYC-driven lymphomas***

370   Our findings thus far suggested that subversion of NK cell-mediated immune surveillance

371   is critical for MYC-driven lymphomagenesis. Next, we investigated whether NK cells can be

372   developed as an immunotherapy against MYC-driven lymphomas by evaluating the effects of

373   NK cells in MYC-driven lymphoma initiation, and recurrence post MYC inactivation.

374   First, we injected intravenously luciferase-labeled MYC-driven T cell lymphoblasts

375   derived from an *SRα-tTA/tet-O-MYC* mouse (**Supplementary Figure 14**) into recipients with

376   (NOD SCID) or without (NOD SCID IL-2Rγ$^{-/-}$, NSG) NK and other innate lymphoid cells.

377   Lymphoma onset (day 5 for NOD SCID IL-2Rγ$^{-/-}$ and day 18 for NOD SCID, **Figures 7a-b**),

17

378   and median morbidity (day 10 for NOD SCID IL-2Rγ$^{-/-}$ and day 20 for NOD SCID, **Figure 7b**)

379   of mice were significantly delayed in NOD SCID transplant recipients with NK cells. T cell

380   lymphomas eventually engrafted in the bone marrow of NOD SCID mice where NK cells are

381   present (**Figure 7a**). We infer that while NK cell-mediated immune surveillance initially blocks

382   MYC-driven lymphomagenesis, continued MYC expression eventually suppresses NK cells to

383   establish lymphomas, as seen in primary *SRα-tTA/tet-O-MYC* mice.

384   Engraftment of T cell lymphoma at sites with NK cell-mediated surveillance such as the

385   bone marrow (**Figure 7a**, BLI image day 18 post injection) suggested that NK cell-mediated

386   allogeneic rejection is an unlikely explanation for delayed lymphoma engraftment in NOD SCID

387   mice. However, we wanted to definitively rule out this possibility by transplanting syngeneic

388   mature NK cells (CD3$^-$ NKp46$^+$) obtained from healthy normal mice (**Supplementary Figure**

389   **18**) into NSG mice three days before (d-3) T cell lymphoma transplantation (d0) (**Figure 7c**). We

390   observed that T cell lymphoma initiation is significantly delayed in transplant recipients that

391   received syngeneic NK cells in comparison to transplant recipients that received the vehicle

392   control (**Figures 7c-d**). Despite delayed lymphoma initiation in transplant recipients that

393   received NK cells, systemic lymphoma eventually develops consistent with our previous findings

394   that, once established, MYC-driven lymphomas promote NK cell suppression.

395   MYC-driven lymphomas recur post MYC inactivation with 100% penetrance in immune-

396   deficient hosts (NOD SCID IL-2Rγ$^{-/-}$) in comparison to immune-competent hosts where MYC

397   inactivation sustains lymphoma regression [13,51]. We investigated whether NK cells are sufficient

398   to delay lymphoma recurrence post MYC inactivation. Syngeneic NK cells (CD3$^-$ NKp46$^+$) from

399   normal mice when adoptively transferred into T cell lymphoma-bearing NOD SCID IL-2Rγ$^{-/-}$

400   recipients at the time of MYC inactivation delayed lymphoma recurrence (**Figures 7e-f**), and

18

401   prolonged overall survival (**Figure 7g**) when compared to vehicle-treated controls. Thus, NK

402   cells sustain lymphoma regression post MYC inactivation. Collectively, our results suggest that

403   NK cells play an anti-tumorigenic role in MYC-driven lymphoid malignancies, hence making

404   NK cell-based immune therapies as an attractive treatment strategy against MYC-driven

405   lymphomas.

Discussion

406

407   Mapping the perturbation in immune cell subsets during primary tumorigenesis is crucial

408 for identifying immunotherapies that will most effectively treat specific cancers. We employed

409 CyTOF to study the global immune cellular signature of overt MYC-driven T cell lymphomas

410 before and after MYC inactivation (**Figure 1, Supplementary Figures 2-4**). We identified a

411 novel mechanism by which oncogenic MYC oncogene directly suppresses NK cell-mediated

412 immune surveillance. MYC-dependent suppression of NK cells was highly specific since other

413 anti-tumorigenic immune subsets were not altered in numbers by both MYC activation and

414 inactivation (**Figure 1, Supplementary Figures 2-4**). Notably, our results are consistent with a

415 recent report where oncogenic MYC has been shown to promote NK cell exclusion in

416 adenocarcinomas [12]. Our studies provide a novel mechanism by which oncogenic MYC

417 orchestrates such NK exclusion from lymphomas (**Figures 3-5**), illustrate human relevance

418 (**Figure 6**), and demonstrate the therapeutic potential of NK cell adoptive transfers for treating

419 MYC-driven lymphomas (**Figure 7**).

420   We found that mice bearing overt MYC-driven lymphomas have reduced number of NK

421 cells because of a developmental blockade at the NK precursor (NKP) stage that prevents the

422 production of more mature NKp46^{+} iNK cells (**Figure 3**). MYC inactivation significantly

423 reversed this effect. Hence, we conclude MYC-driven lymphomas evade NK cell-mediated

424 immune surveillance by blocking NK cell maturation, and infer that inhibiting MYC is essential

425 for reversing this developmental blockade and eliciting an NK cell-mediated response against

426 "MYC-addicted" tumors. Arrest in NK cell maturation has been demonstrated to be a critical

427 mechanism of immune escape in cancers [26,27]. Our findings demonstrate that the overexpression

428   of oncogenic MYC in malignant lymphocytes orchestrates such arrest in NK cell development in

429   the lymphoma microenvironment.

430   We show that MYC-driven lymphomas evade NK cell-mediated immune surveillance by

431   transcriptionally repressing the STAT1/2-Type I IFN cytokine axis (**Figures 5g-k,**

432   **Supplementary Figure 17**) required for NK cell maturation [29–35]. Malignant lymphocytes

433   overexpressing oncogenic MYC show suppressed production of Type I IFNs (**Figures 5e-f,**

434   **Supplementary Figures 10, 15**). In turn, this blocks the maturation of NK cells in the

435   lymphoma microenvironment. We also found that MYC-driven human lymphomas were

436   associated with concomitant suppression of STAT1/2 and exclusion of NK cells (**Figure 6**).

437   We could restore NK cell production in spleens of lymphoma-bearing mice upon Type I

438   IFN treatment (**Figures 4f-j**). Hence, MYC suppresses the STAT1/2-Type I IFN cascade and

439   blocks NK cell-mediated immune surveillance (**Supplementary Figure 19**). We infer that

440   administration of Type I IFNs can bypass the maturation defect of NK cells and restore NK cell-

441   mediated immune surveillance of MYC-induced hematologic malignancies. In addition to their

442   use as anti-viral agents, Type I IFNs can elicit anti-proliferative effects on cancer cells [33,52]. Our

443   current study explains why MYC-driven B cell lymphoma lines are sensitive to Type I IFN

444   therapy [53], and illustrates new functional roles for Type I IFN therapy in lymphoid malignancies.

445   Prior studies have shown that specific NK cell receptor-ligand interactions mediate the

446   recognition of tumors by NK cells and can block MYC-driven lymphomagenesis [54]. Expression

447   levels of NKG2D (KLRK1) that were reduced *in vivo* in our primary autochthonous model

448   bearing overt lymphoma (MYC^{ON}), were restored to normal levels post MYC inactivation

449   (MYC^{OFF}) (**Figure 4e**), suggesting a possible suppression of NKG2DL on MYC-driven tumor

450   cells. Consistent with a previous study, we observe a transcriptional repression of B2M in MYC-

21

451   driven primary murine lymphomas (MYC^{ON}) in comparison to healthy controls and MYC-

452   inactivated (MYC^{OFF}) lymphomas (**Figure 4e**) [55]. Therefore, multiple mechanisms of MYC-

453   mediated suppression of NK surveillance may be at play during lymphomagenesis.

454   Finally, our results may have implications for cancer immunotherapy [56]. We observed

455   that adoptively transferred NK cells significantly delayed overt MYC-driven lymphomagenesis,

456   and contributed to sustained lymphoma regression post MYC inactivation (**Figure 7**), suggesting

457   that MYC-driven lymphomas may be particularly sensitive to NK cell-based therapies. Most

458   conventional chemotherapies used for lymphoid malignancies are immune suppressive.

459   Therapies that are directed at restoring the immune response may be particularly effective

460   against MYC-driven hematopoietic malignancies. Our findings underscore the importance of

461   identifying MYC inhibitors [57] and combining these with NK cell-based therapies [58] to achieve

462   maximum therapeutic benefit. We suggest that, as others and we investigate potential therapeutic

463   candidates that target MYC, it will be essential to consider the role of NK cell-mediated immune

464   surveillance in defining the modes of therapy; and to identify the characteristics, timing, and

465   dosage of NK cells for maximum therapeutic benefit.

Methods

Cell lines and cell culture

Conditional MYC-driven mouse T cell lymphoma cell lines (**Supplementary Figure 14**) were derived from *SRα-tTA/tet-O-MYC* mice. c-MYC was inhibited in *SRα-tTA/tet-O-MYC* T-lymphoma cells by treating cell cultures with 0.02 µg/ml doxycycline (Sigma-Aldrich, T7660) for 4, 8, 24 and 48h. BL-like human P493-6 cells were kindly provided by Chi Van Dang, University of Pennsylvania. For c-MYC inactivation in P493-6 cells, the conditional p*myc*-tet construct was repressed with 0.1 µg/ml doxycycline (Sigma-Aldrich, T7660) for 24 h. Cell lines were confirmed to be negative for mycoplasma contamination and maintained in Roswell Park Memorial Institute 1640 medium (RPMI, Invitrogen) with GlutaMAX containing 10% fetal bovine serum, 100 IU/ml penicillin, 100 µg/ml streptomycin, 50 mM 2-mercaptoethanol at 37 °C in a humidified incubator with 5% CO_2.

Isolation and processing of immune cells from mice

We used young male mice (around 8-12 weeks of age). The following strains of mice were used: *SRα-tTA/tet-O-MYC* mice and the corresponding FVB/N wildtype strain. The *SRα-tTA/tet-O-MYC* males developed T cell lymphoma at approximately two-three months of age. Diseased mice were identified based on the presence of visible symptoms of T cell lymphoma development; namely, loss of weight and appetite, ruffled fur, shortness of breath and movement difficulties. Half the number of male littermates that developed T cell lymphoma were subjected to doxycycline treatment to inactivate MYC. For T cell lymphoma mice subject to MYC inactivation, one starter dose of doxycycline was given intraperitoneally, after which, the mice continuously received doxycycline for four days in their drinking water. Leukemic littermates

from each cage were randomly and equally divided between MYC$^{ON/HIGH}$ (untreated) or MYC$^{OFF/LOW}$ (doxycycline-treated) groups. Spleens, blood and bone marrow were isolated from the three mice groups, namely, *SRα-tTA/tet-O-MYC* (MYC$^{ON/HIGH}$), *SRα-tTA/tet-O-MYC +* Doxycycline (MYC$^{OFF/LOW}$), and normal healthy (FVB/N) controls. Blood was drawn by cardiac puncture after euthanizing the mice, and directly subjected to erythrocyte lysis. Bone marrow was obtained by flushing the cavities of femur and tibia with PBS. Spleen and bone marrow were homogenized using a $19^{1/2}$G needle and filtered through a 70µm filter. After depletion of erythrocytes from spleen, blood and bone marrow using RBC lysis buffer (BD PharmLyse, BD Biosciences), washed cells were cryopreserved and utilized for CyTOF or flow cytometry. No blinding was done while executing the animal experiments.

Mass cytometry (CyTOF Immunophenotyping)

This assay was performed in the Human Immune Monitoring Center at Stanford University. Mouse splenocytes were thawed in warm media, washed twice, resuspended in CyFACS buffer (PBS supplemented with 2% BSA, 2 mM EDTA, and 0.1% soium azide). Viable cells were then counted by Vicell. Cells were added to a V-bottom microtiter plate at 1 million viable cells/well and washed once by pelleting and resuspension in fresh CyFACS buffer. The cells were stained for 60 min on ice with 50uL of the following antibody-polymer conjugate cocktail (**Supplementary Table 1**). All antibodies were custom-ordered metal-conjugates from Fluidigm (**Supplementary Table 1**). The cells were washed twice; by pelleting and resuspension with 500 uL FACS buffer. The cells were resuspended in 100uL PBS buffer containing 1.7 ug/mL Live-Dead (DOTA-maleimide (Macrocyclics) containing natural-abundance indium). The cells were washed twice by pelleting and resuspension with 500uL CyFACS buffer. The cells

were resuspended in 100uL 2% PFA in PBS and placed at 4°C overnight. The next day, the cells were pelleted and washed by resuspension in fresh PBS. The cells were resuspended in 100uL eBiosciences permeabilization buffer (1x in PBS) and placed on ice for 45 min before washing twice with 500uL CyFACS buffer. The cells were resuspended in 100uL iridium-containing DNA intercalator (1:2000 dilution in PBS; DVS Sciences) and incubated at room temperature for 20 min. The cells were washed once in CyFACS buffer, then three times in 500uL MilliQ water. The cells were diluted to a concentration of ~800,000 cells/mL in MilliQ water containing 0.1x EQ normalization beads (Fluidigm) before injection into the CyTOF (Fluidigm). Data analysis was performed using FlowJo v10 by gating on intact cells based on the Iridium vs Ce140 (bead), then both Iridium isotopes from the intercalator, then on singlets by Ir191 vs cell length, then on live cells (Indium-LiveDead minus population), followed by cell subset-specific gating (**Supplementary Figure 20**). The data was analyzed using FlowJo X 10.0.7r2 and viSNE (Cytobank Inc.).

Phospho-CyTOF

The harvested cells were suspended in 16% PFA and incubated for 10 minutes at room temperature. After washing with CyFACS buffer (1x CyPBS with 0.1% BSA, and 0.05% Na Azide; made in Milli-Q water), surface staining was performed by incubating the cells with the surface-staining antibody cocktail (**Supplementary Table 2**) at room temperature for 30 minutes. The cells were then washed with CyFACS buffer and permeabilized before carrying out intracellular staining. The cells were then incubated with the intracellular antibody cocktail (**Supplementary Table 2**) at room temperature for 30 minutes. After washing with CyPBS, the cells were incubated with Ir-intercalator solution on ice for 20 minutes. The samples were then

washed with Milli-Q water and acquired on the CyTOF instrument using standard instrument set up procedures. The data was analyzed using FlowJo X 10.0.7r2.

Flow cytometry

All antibodies for flow cytometry measurements as well as their respective isotype controls are indicated in **Supplementary Table 3**. Surface staining antibodies that were PE conjugated were used at a dilution of 1:10 and the ones conjugated with FITC and APC at a dilution of 1:5. Multicolor flow cytometry staining was performed according to standard procedures. Cells were stained with Propidium Iodide (PI, Sigma-Aldrich) to gate out dead cells. Labeled cells were analyzed on a FACSCalibur (Becton Dickinson). The data was analyzed using FlowJo X 10.0.7r2. Gating strategy is provided in **Supplementary Figure 20**.

Calculation of absolute immune cell counts

Viable cells were counted using a Vicell before subjecting the single cell suspensions of spleen, blood and bone marrow to CyTOF or flow cytometry, respectively. Using the percentages of the immune populations calculated by CyTOF and flow cytometry on the same day, absolute viable cell numbers of the different immune subsets were computed.

RNA sequencing

A part of the splenic single cell suspensions from normal (FVB/N, n =3), SRα-tTA MYC^{ON} (n = 3) and SRα-tTA MYC^{OFF} (n = 3) mice subjected to CyTOF were used to generate RNA. RNA sequencing was performed at the Beijing Genomics Institute (BGI) using the BGISEQ-500 instrument. The experimental pipeline is described below:

Library Preparation: Oligo (dT) magnetic beads were used to select mRNA with polyA tail, or hybridize the rRNA with DNA probe and digest the DNA/RNA hybrid strand, followed by DNase I reaction to remove DNA probe. After obtaining the target RNA, it was fragmented and reverse transcribed to double-strand cDNA (dscDNA) by N6 random primer. The dscDNA was end repaired with phosphate at 5' end and stickiness 'A' at 3' end. The adaptor with stickiness 'T' at 3' end was ligated to the dscDNA. Two specific primers were used to amplify the ligation product. The PCR product was then denatured and the single strand DNA was cyclized by splint oligo and DNA ligase. Sequencing was then performed on the prepared library.

Bioinformatics Pipeline: Primary sequencing data (raw reads) were subjected to quality control (QC). After QC, raw reads were filtered into clean reads before alignment to the reference sequences. Once alignment passed QC, we proceeded with downstream analysis including gene expression and deep analysis based on gene expression (PCA/correlation/screening differentially expressed genes).

Data Filtering: Data was filtered reads with adaptors, reads with greater than 10% unknown bases and low quality reads.

Reads Mapping: Bowtie 2 was used to map clean reads to reference gene, and HISAT was used to map reads to reference genome (mm8).

Gene Quantification: RSEM was used to compute Maximum likelihood abundance estimates using the Expectation Maximization (EM) algorithm. FPKM method was used to calculate the expression levels of individual genes.

RNA sequencing data are provided in Gene Expression Omnibus (GSE106078).

CIBERSORT

Human CIBERSORT was carried out at https://cibersort.stanford.edu/ using LM22 reference matrix of gene expression in human immune subsets *(19)*. For CIBERSORT of splenic immune compositions in normal (FVB/N), SRα-tTA MYC^{ON} and SRα-tTA MYC^{OFF} mice, a reference matrix was generated using ImmGen (https://www.immgen.org/, GSE15907). CIBERSORT was carried out on CyTOF-matched normal (n =3), SRα-tTA MYC^{ON} (n = 3) and SRα-tTA MYC^{OFF} (n = 3) samples.

Transplantation of MYC-addicted T cell lymphoma and bioluminescence imaging

A MYC-addicted T cell lymphoma cell line derived from a male *SRα-tTA/tet-O-MYC* mouse (**Supplementary Figure 14**) was labeled with luciferase. 3 X 10^6 luciferase-labeled T cell lymphoma cells were then injected intravenously into two groups of immune-deficient hosts: NOD SCID (The Jackson Laboratory) and NOD-SCIDIL-2R$\gamma^{-/-}$ (NSG). Male transplant recipients used were between 4-5 weeks of age. Leukemic engraftment and progression were tracked by bioluminescence imaging (BLI) of the transplant recipients twice every week using an *in vivo* IVIS 100 bioluminescence/optical imaging system (Xenogen). D-Luciferin (Promega) dissolved in PBS was injected intraperitoneally at a dose of 2.5 mg per mouse 15 min before measuring the luminescence signal. General anesthesia was induced with 3% isoflurane and continued during the procedure with 2% isoflurane introduced through a nose cone. No blinding was done while executing the animal experiments. All mouse experiments were approved by the Administrative Panel on Laboratory Animal Care (APLAC) at Stanford University, and were carried out in accordance with institutional and national guidelines.

Adoptive transfer of NK cells into T cell lymphoma-bearing recipient mice

3×10^6 luciferase-labeled T cell lymphoma cells were injected intravenously into 4-8 week old NSG mice (n=19). Post verification of T cell lymphoma engraftment by BLI, all mice were treated with doxycycline to inactivate MYC. 10 of the 19 mice were subjected to adoptive transfer of NK cells isolated from spleens of 4-8 week old FVB/N mice by magnetic activated cell sorting (MACS, NK Cell Isolation Kit II, Miltenyi Biotech). Flow cytometry was performed to confirm the purity of the isolated NK cells. 1×10^6 MACS purified NK cells were injected per mouse into NSG transplant recipients bearing regressed T cell lymphoma (on doxycycline, MYC^{OFF}).

Type I IFN treatment of primary *SRα-tTA/tet-O-MYC* mice

20,000U of Type I IFNα (R&D systems) was administered intraperitoneally to SRα-*tTA/tet-O-MYC* mice bearing overt lymphoma for 3 days. On day 3, spleens from treated mice were collected, and subjected to flow cytometry for NK and T cells. PBS-treated mice were used as controls. Absolute cell counts were obtained as described previously.

Immunoblotting

Cells were lysed in CelLytic buffer (Sigma) supplemented with 1% protease inhibitor 'cocktail' (Pierce). Protein samples were subsequently separated by electrophoresis through NuPAGE (Invitrogen) 4–12% Bis-Tris gradient gels and were transferred to PVDF membranes (Immobilion; Millipore). For the detection of mouse and human proteins by immunoblot analysis, we used primary antibodies together with the WesternBreeze immunodetection system (Invitrogen). All antibodies used for immunoblotting and their corresponding dilutions are given in **Supplementary Table 4**.

Retrovirus production and transduction

Transfection of retroviral constructs (**Supplementary Table 5**) was performed using Lipofectamine 2000 (Invitrogen) with Opti-MEM media (Invitrogen). Retroviral supernatants for infection of cells were generated after co-transfection of Phoenix cells containing the plasmids pHIT60 (gag-pol) and pHIT123 (ecotropic envelope) (provided by G.P. Nolan), with the retroviral constructs. Cells were cultured in high-glucose DMEM (Invitrogen) with GlutaMAX containing 10% FBS, 100 IU/ml penicillin, 100 μg/ml streptomycin, 25 mM HEPES, pH 7.2, 1 mM sodium pyruvate and 0.1 mM nonessential amino acids. Serum-free medium was replaced after 16 h with growth medium containing 10 mM sodium butyrate. After 8 h of incubation, the medium was changed back to growth medium without sodium butyrate. 24 h later, we harvested the viral supernatants, passed them through a 0.45-μm filter, and centrifuged them twice at 2,000g for 90 min at 32 °C on 50 μg/ml RetroNectin-coated non–tissue-culture-treated six-well plates. Pre-B cells (2×10^6 to 3×10^6 cells per well) were transduced by centrifugation at 600g for 30 min and were maintained overnight at 37 °C with 5% CO_2 before transfer into culture flasks.

Lentivirus production and transduction

Lentiviral (**Supplementary Table 5**) transfections were performed using Lipofectamine 2000 (Invitrogen) with Opti-MEM media (Invitrogen). We produced lentiviral supernatants to infect murine cells by cotransfecting HEK 293FT cells with the plasmids psPAX2 (gag-pol; Didier Trono, Addgene 12260) and pMD2.G (VSV-G envelope; Didier Trono, Addgene 12259). Cells were cultivated in high-glucose DMEM (Invitrogen) with GlutaMAX as described above.

Culture supernatants were concentrated with Lenti-X™ Concentrator (Clontech) according to the manufactures recommendation. The concentrated viruses were incubated with the cells for 50 µg/ml RetroNectin-coated non- tissue culture treated 6-well plates.

Quantitative RT-PCR

Quantitative real-time PCR carried out with the SYBRGreenER mix from Invitrogen according to standard PCR conditions and an ABI7900HT real-time PCR system (Applied Biosystems). Primers for quantitative RT-PCR are in **Supplementary Table 6**.

Immunohistochemistry

Spleens and thymuses obtained from experimental mice were immersed in 20 ml of formalin (VWR) for 24h and transferred to PBS. Paraffin embedding was carried out using standard procedures on a Tissue-TEK VIP processor (Miles Scientific), and 4µm sections were mounted on Apex superior adhesive slides (Leica Microsystems) and stained on a Ventana BenchMark automated IHC stainer). Immunohistochemistry sections were mounted with mounting medium, antifade reagent (Pro-Long Gold; Invitrogen) was applied, and coverslips were sealed before acquisition of images at 25°C on a Zeiss Axiovert 200M inverted confocal microscope with a 40 Plan Neofluor objective using IP Lab 4.0 software (Scanalytics).

ChIP-sequencing analysis

Raw ChIP-sequencing files were downloaded from Gene Expression Omnibus (GEO). The FASTQ Groomer in Galaxy Software (https://usegalaxy.org/) was used to generate files that

were mapped to RefSeq database for mouse genes (mm9). The resulting bigWig files processed from Galaxy were visualized in Integrated Genome Viewer (IGV_2.3.72).

Statistical analysis

CyTOF, flow cytometry and CIBERSORT results are shown as box plots and comparisons between any two groups were made using the Mann-Whitney U test (not assuming normal distributions) with Graphpad Prism software. All remaining data are presented as mean ± s.d. The comparisons for the mean values between two sample groups were made using the two-tailed Student's *t*-test after calculating variances for each group with Graphpad Prism software. For experiments involving transplantation of cells into mice, the minimal number of mice in each group was calculated through the use of the 'cpower' function in the R/Hmisc package (R Development Core Team 2009; http://www.r-project.org). The Kaplan-Meier method was used for estimation of overall survival and relapse-free survival. For all survival analyses, the log-rank test was used to compare groups of transplanted mice or human patients. The R package 'survival' version 2.35-8 was used for the survival analysis. All p-values are two-tailed. The level of significance was set at $P < 0.05$. P-values: ns = non- significant; *p < 0.05; **p < 0.01; ***p < 0.001; ****p < 0.0001.

Institutional Approval

All mouse experiments were approved by the Administrative Panel on Laboratory Animal Care (APLAC) at Stanford University, and were carried out in accordance with institutional and national guidelines.

References

1. Felsher, D. W. & Bishop, J. M. Reversible tumorigenesis by MYC in hematopoietic lineages. *Mol. Cell* **4,** 199–207 (1999).

2. Weinstein, I. B. Cancer. Addiction to oncogenes--the Achilles heal of cancer. *Science* **297,** 63–64 (2002).

3. Felsher, D. W. Cancer revoked: oncogenes as therapeutic targets. *Nat. Rev. Cancer* **3,** 375–380 (2003).

4. Jain, M. *et al.* Sustained loss of a neoplastic phenotype by brief inactivation of MYC. *Science* **297,** 102–104 (2002).

5. Letai, A. G. Diagnosing and exploiting cancer's addiction to blocks in apoptosis. *Nat. Rev. Cancer* **8,** 121–132 (2008).

6. Goldman, J. M. & Melo, J. V. Chronic myeloid leukemia--advances in biology and new approaches to treatment. *N. Engl. J. Med.* **349,** 1451–1464 (2003).

7. Druker, B. J. *et al.* Efficacy and safety of a specific inhibitor of the BCR-ABL tyrosine kinase in chronic myeloid leukemia. *N. Engl. J. Med.* **344,** 1031–1037 (2001).

8. Sharma, S. V. & Settleman, J. Oncogene addiction: setting the stage for molecularly targeted cancer therapy. *Genes Dev.* **21,** 3214–3231 (2007).

9. Ancrile, B., Lim, K.-H. & Counter, C. M. Oncogenic Ras-induced secretion of IL6 is required for tumorigenesis. *Genes Dev.* **21,** 1714–1719 (2007).

10. Borrello, M. G. *et al.* Induction of a proinflammatory program in normal human thyrocytes by the RET/PTC1 oncogene. *Proc. Natl. Acad. Sci. U. S. A.* **102,** 14825–14830 (2005).

11. Casey, S. C. *et al.* MYC regulates the antitumor immune response through CD47 and PD-L1. *Science* **352,** 227–231 (2016).

12. Kortlever, R. M. *et al.* Myc Cooperates with Ras by Programming Inflammation and Immune Suppression. *Cell* **171,** 1301–1315.e14 (2017).

13. Rakhra, K. *et al.* CD4(+) T cells contribute to the remodeling of the microenvironment required for sustained tumor regression upon oncogene inactivation. *Cancer Cell* **18,** 485–498 (2010).

14. Reimann, M. *et al.* Tumor stroma-derived TGF-beta limits myc-driven lymphomagenesis via Suv39h1-dependent senescence. *Cancer Cell* **17,** 262–272 (2010).

15. Sparmann, A. & Bar-Sagi, D. Ras-induced interleukin-8 expression plays a critical role in tumor growth and angiogenesis. *Cancer Cell* **6,** 447–458 (2004).

16. Topper, M. J. *et al.* Epigenetic Therapy Ties MYC Depletion to Reversing Immune Evasion and Treating Lung Cancer. *Cell* **171,** 1284–1300.e21 (2017).

17. Spitzer, M. H. *et al.* IMMUNOLOGY. An interactive reference framework for modeling a dynamic immune system. *Science* **349,** 1259425 (2015).

18. Rehm, A. *et al.* Dendritic cell-mediated survival signals in Eμ-Myc B-cell lymphoma depend on the transcription factor C/EBPβ. *Nat. Commun.* **5,** 5057 (2014).

19. Hirz, T. *et al.* Neutrophils protect lymphoma cells against cytotoxic and targeted therapies through CD11b/ICAM-1 binding. *Oncotarget* **8,** 72818–72834 (2017).

20. Pylaeva, E., Lang, S. & Jablonska, J. The Essential Role of Type I Interferons in Differentiation and Activation of Tumor-Associated Neutrophils. *Front. Immunol.* **7,** (2016).

21. Walzer, T. *et al.* Identification, activation, and selective in vivo ablation of mouse NK cells via NKp46. *Proc. Natl. Acad. Sci. U. S. A.* **104,** 3384–3389 (2007).

22. Newman, A. M. *et al.* Robust enumeration of cell subsets from tissue expression profiles. *Nat. Methods* **12,** 453–457 (2015).

24

23. Delgado, M. D. & León, J. Myc Roles in Hematopoiesis and Leukemia. *Genes Cancer* **1,** 605–616 (2010).

24. Huntington, N. D., Vosshenrich, C. A. J. & Di Santo, J. P. Developmental pathways that generate natural-killer-cell diversity in mice and humans. *Nat. Rev. Immunol.* **7,** 703–714 (2007).

25. Yu, J., Freud, A. G. & Caligiuri, M. A. Location and cellular stages of natural killer cell development. *Trends Immunol.* **34,** 573–582 (2013).

26. Mundy-Bosse, B. L. *et al.* MicroRNA-29b mediates altered innate immune development in acute leukemia. *J. Clin. Invest.* **126,** 4404–4416 (2016).

27. Scoville, S. D. *et al.* Human AML activates the AHR pathway to impair NK cell development and function. *Blood* (2018). doi:10.1182/blood-2018-03-838474

28. Wang, F. *et al.* Disruption of Erk-dependent type I interferon induction breaks the myxoma virus species barrier. *Nat. Immunol.* **5,** 1266–1274 (2004).

29. Swann, J. B. *et al.* Type I IFN contributes to NK cell homeostasis, activation, and antitumor function. *J. Immunol. Baltim. Md 1950* **178,** 7540–7549 (2007).

30. Guan, J. *et al.* Role of Type I Interferon Receptor Signaling on NK Cell Development and Functions. *PLOS ONE* **9,** e111302 (2014).

31. Dunn, G. P., Koebel, C. M. & Schreiber, R. D. Interferons, immunity and cancer immunoediting. *Nat. Rev. Immunol.* **6,** 836–848 (2006).

32. Madera, S. *et al.* Type I IFN promotes NK cell expansion during viral infection by protecting NK cells against fratricide. *J. Exp. Med.* **213,** 225–233 (2016).

33. Zitvogel, L., Galluzzi, L., Kepp, O., Smyth, M. J. & Kroemer, G. Type I interferons in anticancer immunity. *Nat. Rev. Immunol.* **15,** 405–414 (2015).

34. Müller, L., Aigner, P. & Stoiber, D. Type I Interferons and Natural Killer Cell Regulation in Cancer. *Front. Immunol.* **8,** (2017).

35. Mizutani, T. *et al.* Conditional IFNAR1 ablation reveals distinct requirements of Type I IFN signaling for NK cell maturation and tumor surveillance. *OncoImmunology* **1,** 1027–1037 (2012).

36. Sabò, A. *et al.* Selective transcriptional regulation by Myc in cellular growth control and lymphomagenesis. *Nature* **511,** 488–492 (2014).

37. Schuhmacher, M. *et al.* The transcriptional program of a human B cell line in response to Myc. *Nucleic Acids Res.* **29,** 397–406 (2001).

38. Staller, P. *et al.* Repression of p15INK4b expression by Myc through association with Miz-1. *Nat. Cell Biol.* **3,** 392–399 (2001).

39. Wanzel, M. *et al.* A ribosomal protein L23-nucleophosmin circuit coordinates Mizl function with cell growth. *Nat. Cell Biol.* **10,** 1051–1061 (2008).

40. Gartel, A. L. *et al.* Myc represses the p21(WAF1/CIP1) promoter and interacts with Sp1/Sp3. *Proc. Natl. Acad. Sci.* **98,** 4510–4515 (2001).

41. Schlee, M. *et al.* c-MYC activation impairs the NF-κB and the interferon response: Implications for the pathogenesis of Burkitt's lymphoma. *Int. J. Cancer* **120,** 1387–1395 (2007).

42. Hummel, M. *et al.* A biologic definition of Burkitt's lymphoma from transcriptional and genomic profiling. *N. Engl. J. Med.* **354,** 2419–2430 (2006).

43. Zech, L., Haglund, U., Nilsson, K. & Klein, G. Characteristic chromosomal abnormalities in biopsies and lymphoid-cell lines from patients with Burkitt and non-Burkitt lymphomas. *Int. J. Cancer* **17,** 47–56 (1976).

44. Peirs, S. *et al.* ABT-199 mediated inhibition of BCL-2 as a novel therapeutic strategy in T-cell acute lymphoblastic leukemia. *Blood* **124,** 3738–3747 (2014).

45. Clappier, E. *et al.* Clonal selection in xenografted human T cell acute lymphoblastic leukemia recapitulates gain of malignancy at relapse. *J. Exp. Med.* **208,** 653–661 (2011).

46. Van Vlierberghe, P., Pieters, R., Beverloo, H. B. & Meijerink, J. P. P. Molecular-genetic insights in paediatric T-cell acute lymphoblastic leukaemia. *Br. J. Haematol.* **143,** 153–168 (2008).

47. Aifantis, I., Raetz, E. & Buonamici, S. Molecular pathogenesis of T-cell leukaemia and lymphoma. *Nat. Rev. Immunol.* **8,** 380–390 (2008).

48. Tremblay, C. S., Hoang, T. & Hoang, T. Early T cell differentiation lessons from T-cell acute lymphoblastic leukemia. *Prog. Mol. Biol. Transl. Sci.* **92,** 121–156 (2010).

49. Gerby, B. *et al.* High-throughput screening in niche-based assay identifies compounds to target preleukemic stem cells. *J. Clin. Invest.* **126,** 4569–4584 (2016).

50. Weng, A. P. *et al.* c-Myc is an important direct target of Notch1 in T-cell acute lymphoblastic leukemia/lymphoma. *Genes Dev.* **20,** 2096–2109 (2006).

51. Choi, P. S. *et al.* Lymphomas that recur after MYC suppression continue to exhibit oncogene addiction. *Proc. Natl. Acad. Sci. U. S. A.* **108,** 17432–17437 (2011).

52. Gajewski, T. F. & Corrales, L. New perspectives on type I IFNs in cancer. *Cytokine Growth Factor Rev.* **26,** 175–178 (2015).

53. Felsher, D. W., Rhim, S. H. & Braun, J. A murine model for B-cell lymphomagenesis in immunocompromised hosts: natural killer cells are an important component of host resistance to premalignant B-cell lines. *Cancer Res.* **50,** 7050–7056 (1990).

54. Belting, L. *et al.* Critical role of the NKG2D receptor for NK cell-mediated control and immune escape of B-cell lymphoma. *Eur. J. Immunol.* **45,** 2593–2601 (2015).

55. Challa-Malladi, M. *et al.* Combined genetic inactivation of β2-Microglobulin and CD58 reveals frequent escape from immune recognition in diffuse large B cell lymphoma. *Cancer Cell* **20,** 728–740 (2011).

56. Zou, W. Mechanistic insights into cancer immunity and immunotherapy. *Cell. Mol. Immunol.* **15,** 419–420 (2018).

57. Delmore, J. E. *et al.* BET bromodomain inhibition as a therapeutic strategy to target c-Myc. *Cell* **146,** 904–917 (2011).

58. Cheng, M., Chen, Y., Xiao, W., Sun, R. & Tian, Z. NK cell-based immunotherapy for malignant diseases. *Cell. Mol. Immunol.* **10,** 230–252 (2013).

Author Contributions

S.S. and D.W.F. conceived the study. S.S. developed the experimental methodology and conducted most of the experiments. L.D.H., D.F.L., A.D., C.H., A.M., and M.L. performed experiments. R.D. helped with analysis and interpretation of RNA sequencing results. S.S. wrote the manuscript. D.W.F. and H.T.M. provided helpful scientific input on the manuscript. H.T.M., and D.W.F. helped in editing the manuscript. H.T.M and D.W.F. provided administrative, technical, and material support. D.W.F. supervised the study.

Conflicts of Interest

The authors declare no potential conflicts of interest.

Figure 1: *NK cells are reduced in numbers and maturation in primary MYC-driven T cell lymphomas*

Figure 1: NK cells are reduced in numbers and maturation in primary MYC-driven T cell lymphomas. (a-e) viSNE of CyTOF data depicting splenic $CD3^+$ T (**a**), splenic $CD4^+$ T (**b**), and $CD8a^+$ T (**c**), $NKp46^+$ NK (**d**), and $CD19^+$ B (**e**) cell compositions of one representative mouse from normal (n = 11), SRα-tTA MYC^{ON} (n = 9), and SRα-tTA MYC^{OFF} (doxycycline 96 h, n = 10) groups. **(f-i)** Quantification of absolute counts of total WBC (**f**), immature $CD3^+$ $CD8^+$ $CD4^+$ DP lymphoma T cells (**g**), $CD3^-$ $NKp46^+$ mature NK (**h**), and $CD19^+$ B (**i**) cells in normal (n = 11), SRα-tTA MYC^{ON} (n = 9), and SRα-tTA MYC^{OFF} (doxycycline 96 h, n = 10) mice subjected to CyTOF. (**j**) Median fluorescence intensity (MFI) of NKp46 on splenic NK cells from normal (n = 11), SRα-tTA MYC^{ON} (n = 9), and SRα-tTA MYC^{OFF} (doxycycline 96 h, n = 10) mice. **(k)** Schematic depicting the reversible phenomenon of NK cell (blue) suppression in MYC-driven lymphomas (red). P-values have been calculated using the Mann-Whitney test. P-values: ns = not significant; *p < 0.05; **p < 0.01; ***p < 0.001; ****p < 0.0001.

Figure 2: *NK cell suppression in MYC-driven lymphomas is systemic and depends on MYC status*
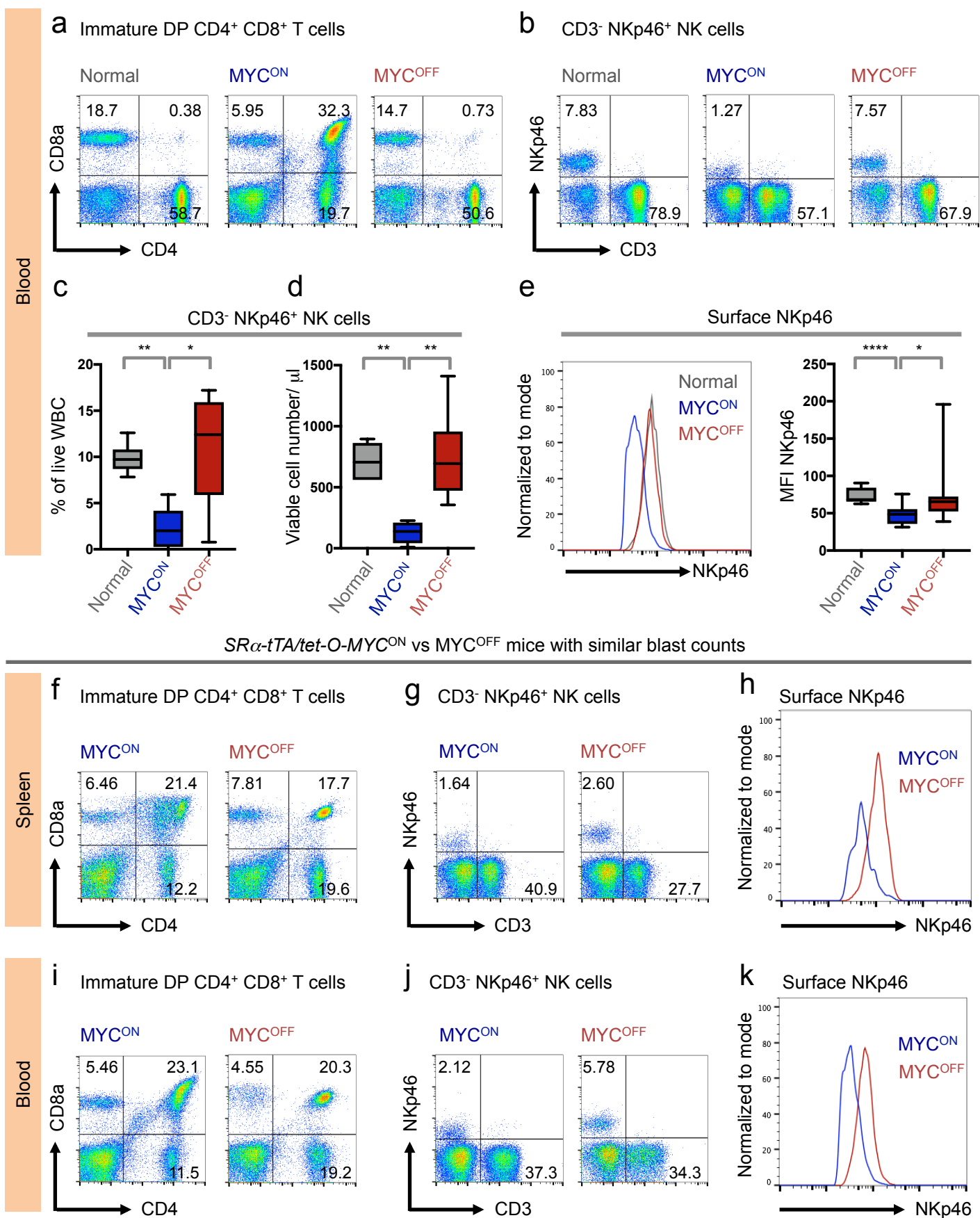
Figure 2: NK cell suppression in MYC-driven lymphomas is systemic and depends on MYC status. (a-b) Representative flow cytometry plots depicting percentages of circulating immature CD4$^+$ CD8$^+$ T (**a**), and CD3$^-$ NKp46$^+$ NK (**b**) cells in normal (n = 6), SRα-tTA MYC^{ON} (n = 6), and SRα-tTA MYC^{OFF} (doxycycline 96 h, n = 6) mice. **(c-d)** Quantification of percentages (**c**), and absolute counts per µl of blood (**d**) of CD3$^-$ NKp46$^+$ NK cells, in normal (n = 6), SRα-tTA MYC^{ON} (n = 6), and SRα-tTA MYC^{OFF} (doxycycline 96 h, n = 6) mice. **(e)** Comparison of MFI of surface NKp46 on circulating NK cells in normal (n = 6), SRα-tTA MYC^{ON} (n = 6), and SRα-tTA MYC^{OFF} (doxycycline 96 h, n = 6) mice. **(f-g)** Representative flow cytometry plots depicting percentages of splenic immature CD4$^+$ CD8$^+$ T (**f**), and CD3$^-$ NKp46$^+$ NK (**g**) cells in SRα-tTA MYC^{ON} and SRα-tTA MYC^{OFF} (doxycycline 96 h) mice with comparable blast counts. **(h)** Comparison of surface NKp46 levels (MFI) on splenic NK cells from SRα-tTA MYC^{ON} and SRα-tTA MYC^{OFF} (doxycycline 96 h) mice with comparable blast counts. **(i-j)** Representative flow cytometry plots depicting percentages of circulating immature CD4$^+$ CD8$^+$ T (**i**), and CD3$^-$ NKp46$^+$ NK (**j**) cells in SRα-tTA MYC^{ON} and SRα-tTA MYC^{OFF} (doxycycline 96 h) mice with comparable blast counts. **(k)** Comparison of surface NKp46 levels (MFI) on circulating NK cells from SRα-tTA MYC^{ON} and SRα-tTA MYC^{OFF} (doxycycline 96 h) mice with comparable blast counts. P-values have been calculated using the Mann-Whitney test. P-values: ns = not significant; *p < 0.05; **p < 0.01; ****p < 0.0001.

**Figure 3:**   *Maturation of NK cells is arrested in mice bearing overt MYC-driven T cell lymphomas*
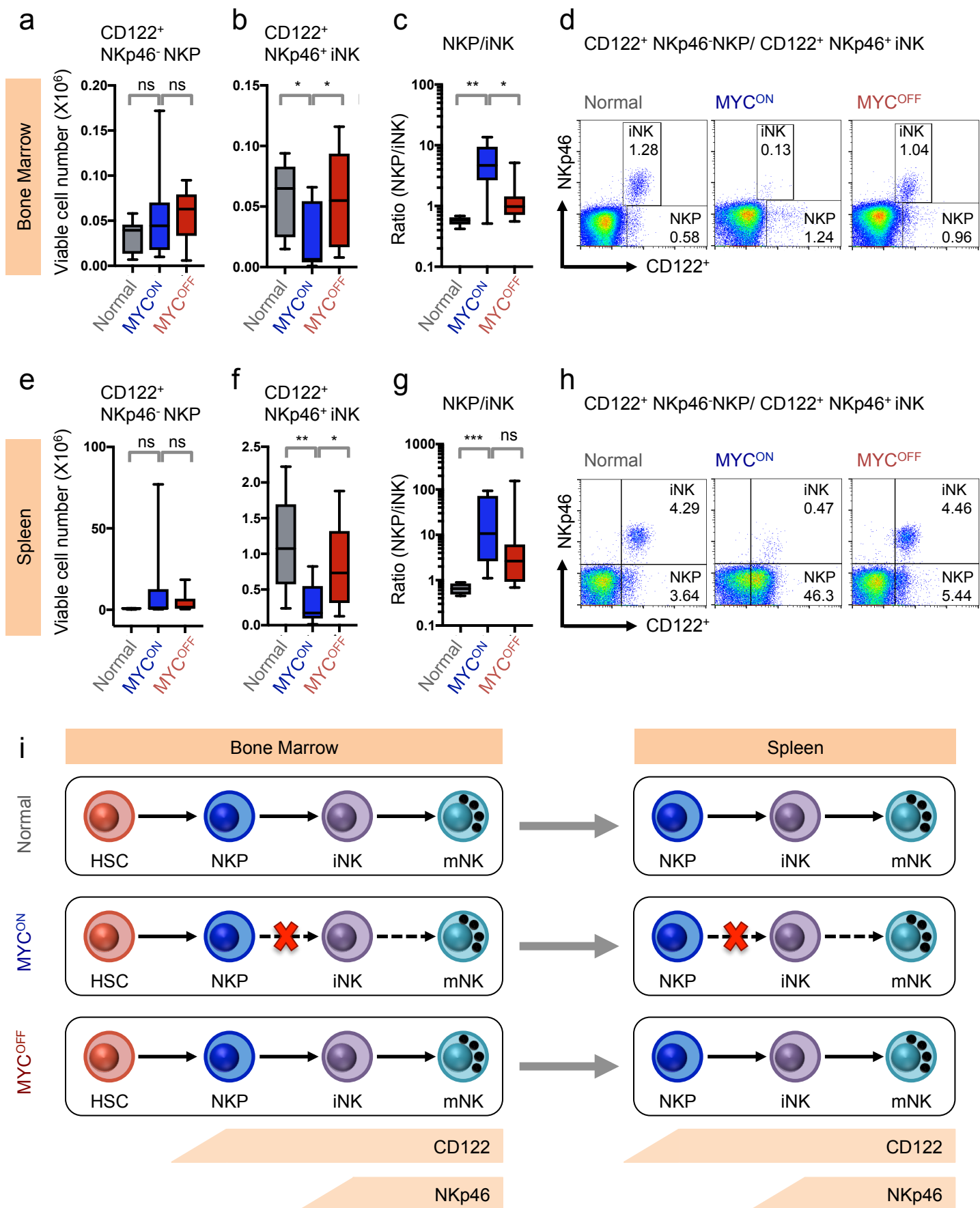
Figure 3: Maturation of NK cells is arrested in mice bearing overt MYC-driven T cell lymphomas. (a-b) Quantification of viable cell numbers of NK precursor cells (NKP, CD122$^+$ NKp46$^-$, (**a**)), and immature NK cells (iNK, CD122$^+$ NKp46$^+$, (**b**)) in normal (n = 8), SRα-tTA MYC^{ON} (n = 8), and SRα-tTA MYC^{OFF} (doxycycline 96 h, n = 8) bone marrow measured by flow cytometry. **(c)** Comparison of proportions of numbers of NKP and iNK cells (NKP/iNK) between normal (n = 8), SRα-tTA MYC^{ON} (n = 8), and SRα-tTA MYC^{OFF} (doxycycline 96 h, n = 8) bone marrow. **(d)** Representative flow cytometry plots depicting NK precursor cells (NKP, CD122$^+$ NKp46$^-$), and immature NK cells (iNK, CD122$^+$ NKp46$^+$) in normal (n = 8), SRα-tTA MYC^{ON} (n = 8), and SRα-tTA MYC^{OFF} (doxycycline 96 h, n = 8) bone marrow. **(e-f)** Quantification of viable cell numbers of NK precursor cells (NKP, CD122$^+$ NKp46$^-$, (**d**)), and immature NK cells (iNK, CD122$^+$ NKp46$^+$, (**e**)) in normal (n = 8), SRα-tTA MYC^{ON} (n = 8), and SRα-tTA MYC^{OFF} (doxycycline 96 h, n = 8) spleens measured by flow cytometry. **(g)** Comparison of proportions of numbers of NKP and iNK cells (NKP/iNK) between normal (n = 8), SRα-tTA MYC^{ON} (n = 8), and SRα-tTA MYC^{OFF} (doxycycline 96 h, n = 8) spleens. **(h)** Representative flow cytometry plots depicting NK precursor cells (NKP, CD122$^+$ NKp46$^-$), and immature NK cells (iNK, CD122$^+$ NKp46$^+$) in normal (n = 8), SRα-tTA MYC^{ON} (n = 8), and SRα-tTA MYC^{OFF} (doxycycline 96 h, n = 8) bone marrow. **(i)** Model depicting the arrest in differentiation from NK precursor (NKP) stage to immature NK (iNK) stage during MYC-driven lymphomagenesis. Arrested step in NK cell differentiation is indicated by a red cross. Dashed arrows indicate stages of NK cell differentiation that do not occur because of the arrest. All p values have been calculated using Mann-Whitney test. P-values: ns = not significant; *p < 0.05; **p < 0.01; ***p < 0.001.

Figure 4: *Escape from NK surveillance during MYC-driven lymphomagenesis is mediated by suppression of Type I IFN signaling*
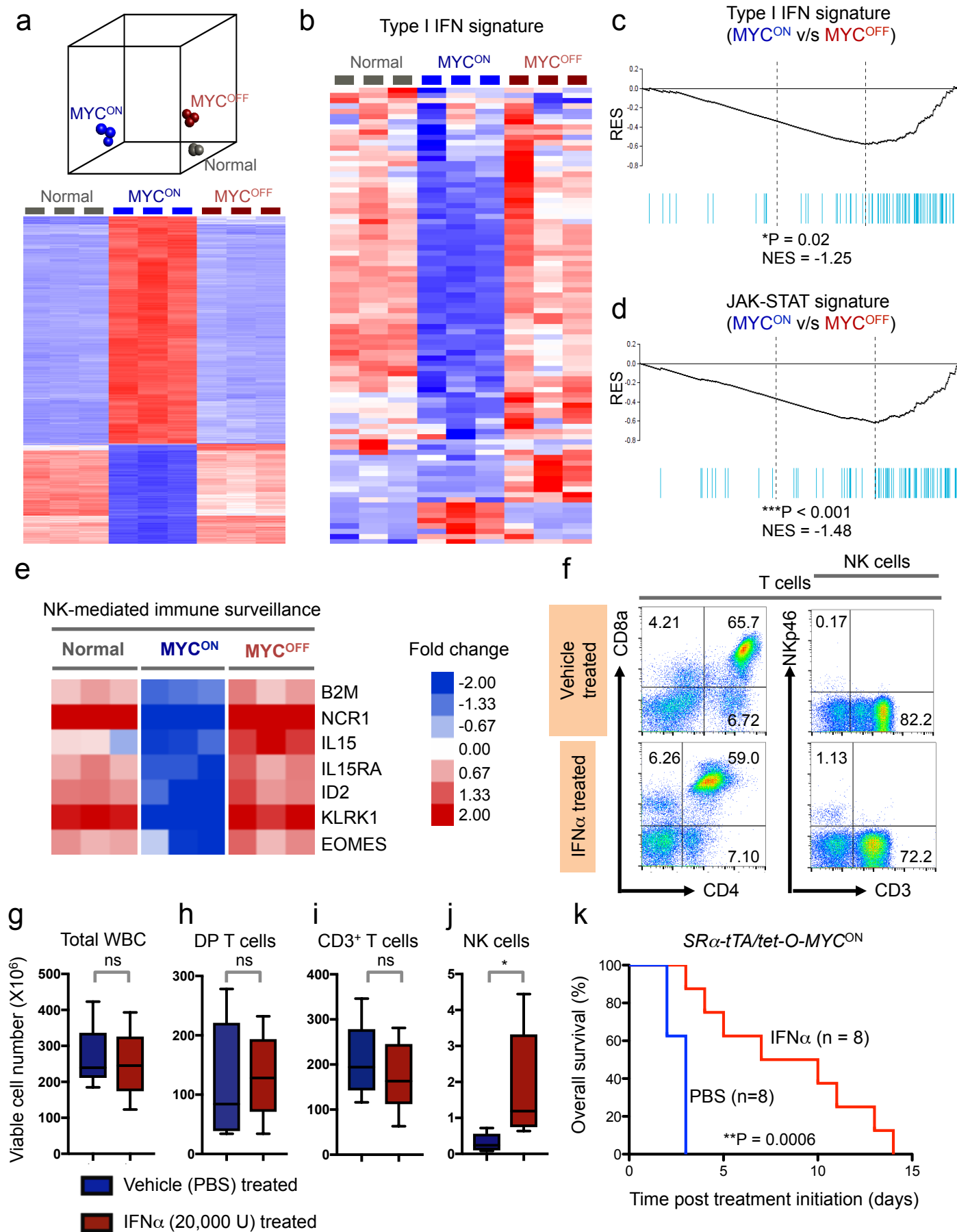
Figure 4: Escape from NK surveillance during MYC-driven lymphomagenesis is mediated by suppression of Type I IFN signaling. (a) Principal component analysis (PCA, top) and heatmap (bottom) depicting global transcriptomic profiles of bulk splenic samples derived from normal (n = 3), SRα-tTA MYC^{ON} (n = 3) and SRα-tTA MYC^{OFF} (n = 3) mice, obtained by RNA sequencing (GSE106078). **(b)** Heatmap showing suppression of Type I IFN signaling in spleens of SRα-tTA MYC^{ON} (n = 3) mice when compared to normal (n =3) and SRα-tTA MYC^{OFF} (n = 3) mice. **(c)** Gene Set Enrichment Analysis (GSEA) depicting suppression of Type I IFN signature in spleens of SRα-tTA MYC^{ON} (n = 3) mice when compared to SRα-tTA MYC^{OFF} (n =3) mice. **(d)** GSEA depicting suppression of JAK-STAT signature in spleens of SRα-tTA MYC^{ON} (n = 3) mice when compared to SRα-tTA MYC^{OFF} (n =3) mice. **(e)** Heatmap comparing expression of key NK cell genes in splenic samples from normal (n = 3), SRα-tTA MYC^{ON} (n = 3) and SRα-tTA MYC^{OFF} (n = 3) mice. **(f)** Representative flow cytometry plots comparing percentages of CD4^{+} CD8^{+} DP T (left) and CD3^{-} NKp46^{+} NK (right) cells between *SRα-tTA/tet-O-MYC* mice in IFNα-treated and vehicle (PBS)-treated groups for three days. **(g-j)** Quantification of absolute counts of total WBC (**g**), CD4^{+} CD8^{+} DP T (**h**), CD3^{+} pan T (**i**), and CD3^{-} NKp46^{+} NK cells (**j**) in *SRα-tTA/tet-O-MYC* mice bearing overt lymphomas (SRα-tTA MYC^{ON}) treated for three days with either IFNα (n = 5), or vehicle (PBS, n = 5). **(k)** Comparison of overall survival (OS) probabilities between PBS (n = 7) and IFNα (n = 7) -treated *SRα-tTA/tet-O-MYC* mice bearing overt lymphomas (SRα-tTA MYC^{ON}, age = 2-3 months). P-values have been calculated using Mann-Whitney test. ns = not significant, *p < 0.05, **p < 0.01.

Figure 5: *MYC transcriptionally represses the STAT1/2-Type I IFN signaling cascade associated with NK cell maturation*
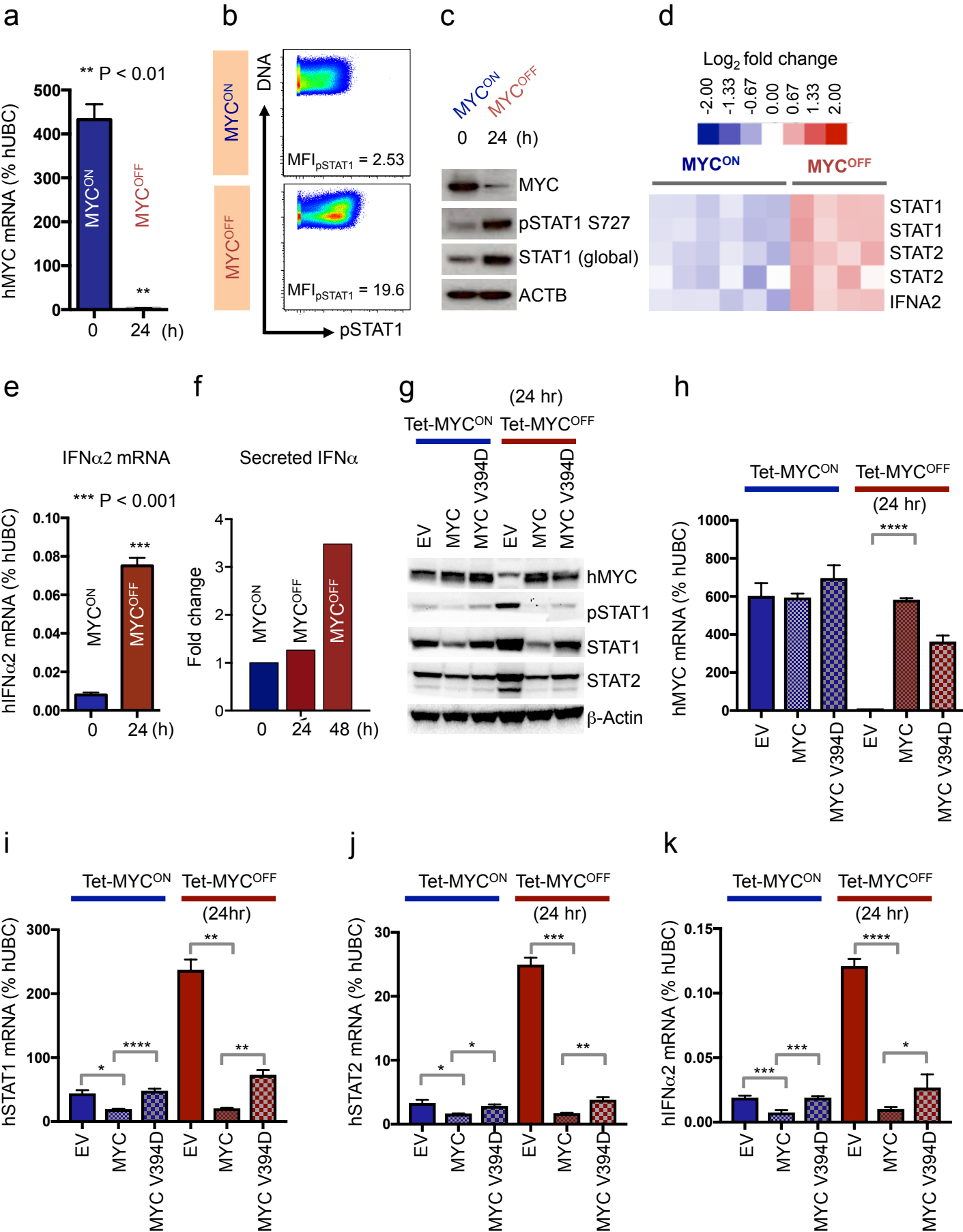
Figure 5: MYC transcriptionally represses the STAT1/2-Type I IFN signaling cascade associated with NK cell maturation. (a) Quantitative real time PCR for MYC in P493-6 BL human cells before and after MYC inhibition for 24h by doxycycline (n = 3, mean ± s.d). **(b)** Phospho mass cytometry (Phospho-CyTOF) depicting changes in pSTAT1 levels before (MYC^{ON}) and after (MYC^{OFF}) MYC inactivation for 24h in P493-6 cells. **(c)** Immunoblotting to validate changes in pSTAT1 observed by phospho-CyTOF. **(d)** Heat map depicting transcriptional changes in STAT1/2-Type I IFN signaling cascade before (MYC^{ON}, n = 6) and after MYC inactivation (MYC^{OFF}, 24h, n = 4) in P493-6 cells using expression arrays. **(e)** Quantitative real time PCR for Type I IFNα2 in P493-6 BL human cells before and after MYC inactivation for 24h by doxycycline (n = 3, mean ± s.d). **(f)** Luminex assay depicting changes in Type I IFNα2 secreted from P493-6 cells before and after MYC inactivation for 24 and 48h. **(g)** Immunoblotting in P493-6 BL cell lines expressing empty vector (EV), MYC overexpression vector (MYC), or a MYC mutant that fails to bind MIZ1 (MYC V394D), pre- (Tet-MYC^{ON}) and post (Tet-MYC^{OFF}) MYC inactivation. **(h-k)** Quantitative real time PCR for MYC (**h**), STAT1 (**i**), STAT2 (**j**), and Type I IFNα2 (**k**) in P493-6 BL cell lines expressing empty vector (EV), MYC overexpression vector (MYC), or a MYC mutant that fails to bind MIZ1 (MYC V394D), pre- (Tet-MYC^{ON}) and post (Tet-MYC^{OFF}) MYC inactivation (n = 3, mean ± s.d). All p values have been calculated using Student's t-test. *p < 0.05; **p < 0.01; ***p < 0.001; ****p < 0.0001.

Figure 6: *MYC^High human lymphomas exhibit decreased levels of STAT1/2 and NK cell-mediated immune surveillance*
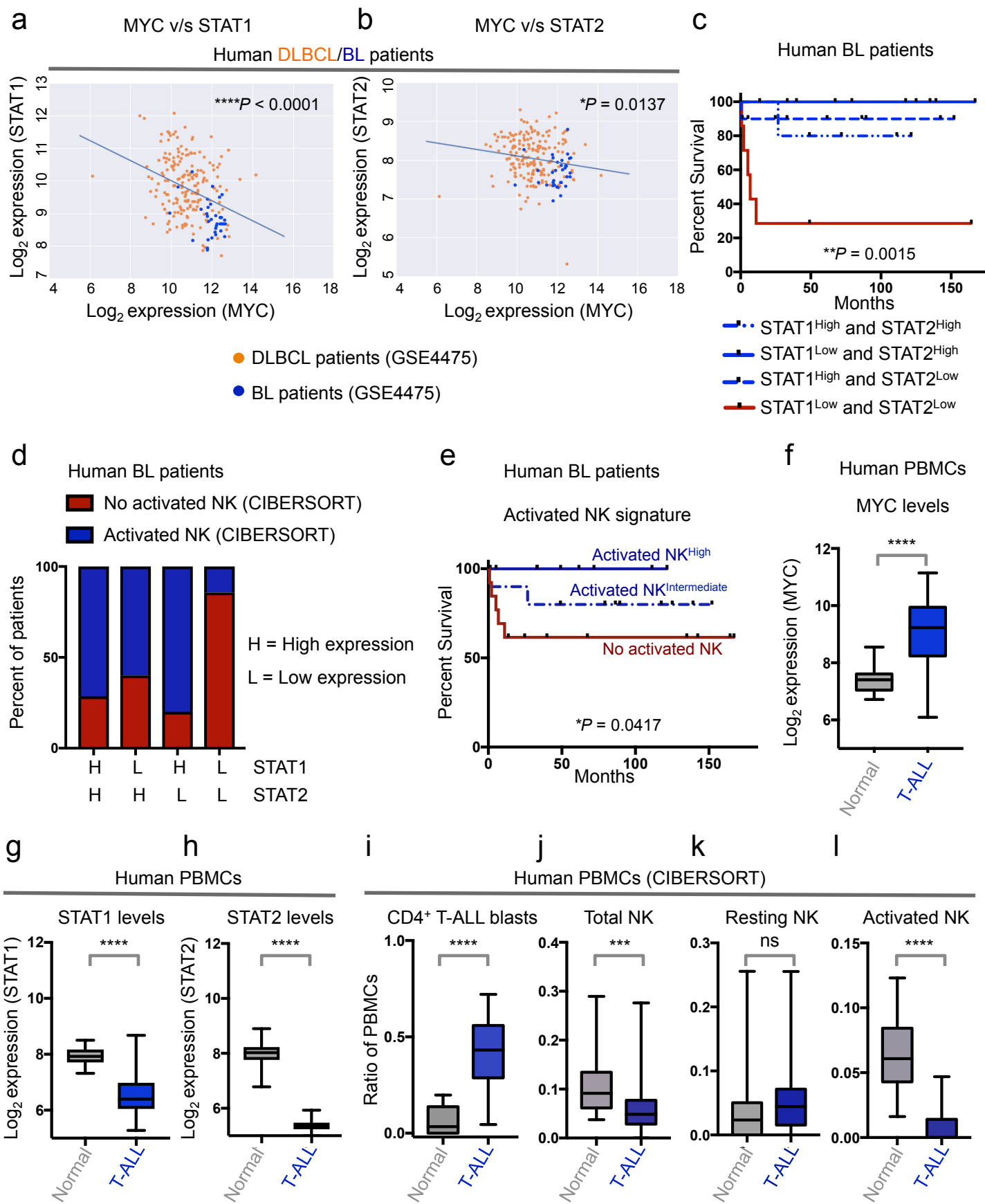
Figure 6: MYC^{High} human lymphomas exhibit decreased levels of STAT1/2 and NK cell-mediated immune surveillance. (a-b) Correlations between mRNA levels of MYC and STAT1 (**a**), or MYC and STAT2 (**b**) in classical MYC-driven human lymphoma patient samples (n = 187, DLBCL, orange; n = 34, BL, blue). (**c**) Multivariate analysis comparing overall survival probabilities of BL patients (n = 34, GSE4475) when divided into 4 groups based on combined levels of STAT1 and STAT2. (**d**) Proportions of patients with no activated NK cells (estimated by CIBERSORT) when BL patients (n = 34, GSE4475) are divided into 4 groups based on combined levels of STAT1 and STAT2. **(e)** Comparison of overall survival probabilities of BL patients (n = 34, GSE4475) separated into three categories based on levels of activated NK cells in the tumor estimated by CIBERSORT, as none (0%, no activated NK), intermediate (Activated NK^{Intermediate}), and high (Activated NK^{High}). **(f-h)** Comparison of mRNA levels of MYC (**f**), STAT1 (**g**), and STAT2 (**h**) in mononuclear cells isolated from healthy human blood (n = 20) and from blood of T-ALL patients (n = 48, GSE62156). **(i-l)** CIBERSORT estimates of relative proportions of T cell blasts (**i**), and NK subsets, namely, total NK (**j**), resting NK (**k**) and activated NK (**l**), in peripheral blood mononuclear cells isolated from healthy individuals (n = 20) and T-ALL patients (n = 48, GSE62156). P-values for all survival analyses have been calculated using the log-rank test. P-values for all other analyses have been calculated using Mann-Whitney test. P-values: ns = not significant; *p < 0.05; **p < 0.01; ****p < 0.0001.

Figure 7: *NK cells slow down growth and recurrence of MYC-driven lymphomas*
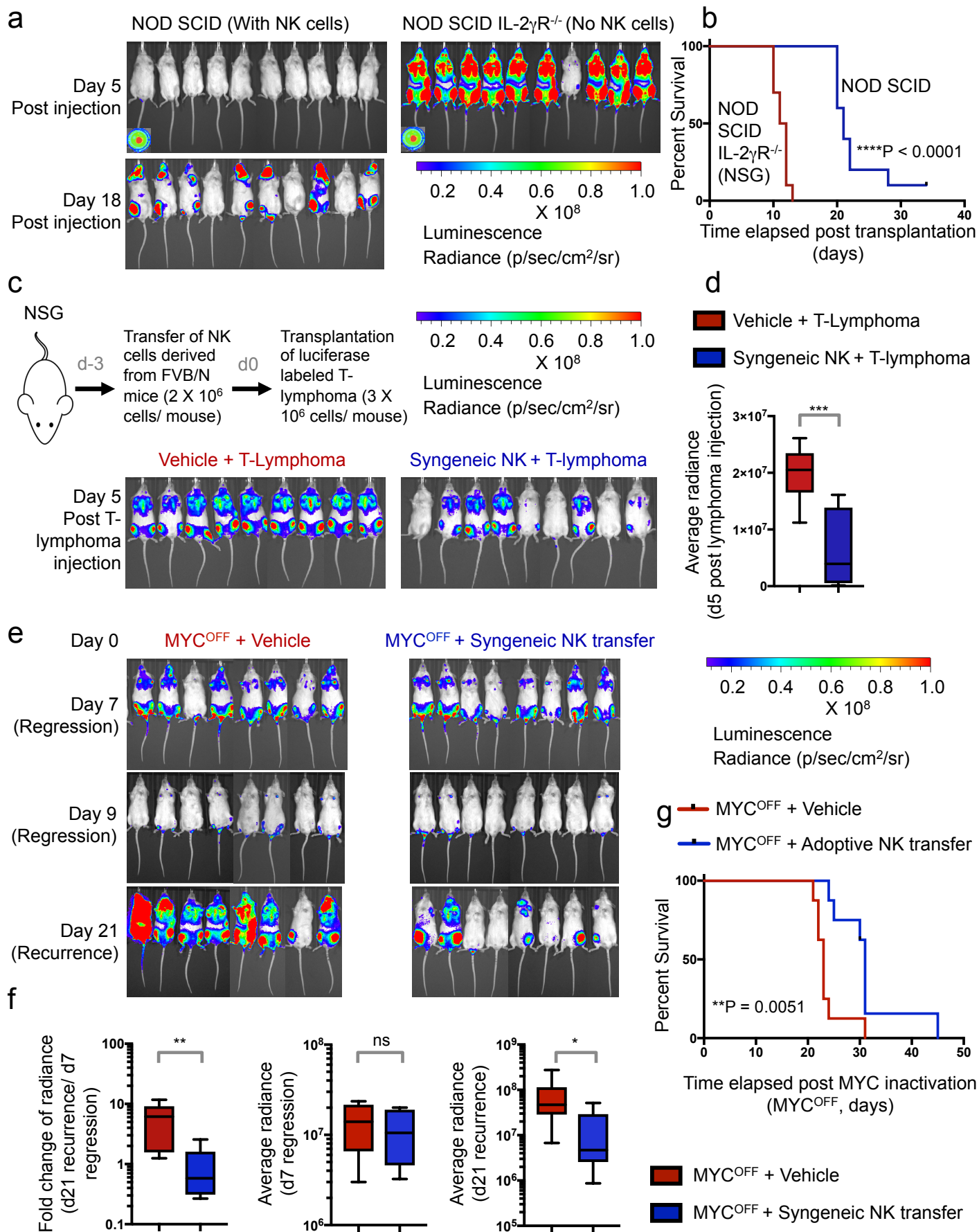
Figure 7: NK cells slow down growth and recurrence of MYC-driven lymphomas. (a) Bioluminescence imaging (BLI) of *NOD-SCID* (n = 10) and *NOD-SCIDIL2R$\gamma^{-/-}$* (n = 10) mice transplanted with SRα-tTA MYC^{ON} mouse T-lymphoma cells post injection to monitor lymphoma engraftment and initiation. **(b)** Comparison of survival probabilities of *NOD-SCID* (n = 10) and *NOD-SCIDIL2R$\gamma^{-/-}$* (NSG, n = 10) T-lymphoma transplant recipients. **(c)** BLI of NSG T cell lymphoma transplant recipients comparing lymphoma engraftment and initiation in the presence (n = 9) and absence (n = 9) of NK cells syngeneic to the tumor. **(d)** Quantification of changes in BLI signal of NSG transplant recipients that received vehicle or syngeneic NK cells before transplantation of T-lymphoma cells. **(e)** BLI of NSG T cell lymphoma transplant recipients comparing recurrence rates upon MYC inactivation in the absence (MYC^{OFF} + vehicle, n = 8) or presence of NK cells (MYC^{OFF} + Adoptive NK transfer, n = 8). **(f)** Quantification of changes in BLI signal (left) and absolute signals (middle and right) at the time of lymphoma regression (d7 MYC^{OFF}) and lymphoma relapse (d21 MYC^{OFF}). **(g)** Comparison of survival probabilities of NSG T-lymphoma transplant recipients that received either vehicle (n = 8) or adoptive NK transfer (n = 8) at the time of MYC inactivation (MYC^{OFF}). P-values for all survival analyses have been calculated using the log-rank test. P-values for all other analyses have been calculated using Mann-Whitney test. P-values: ns = non significant; *p < 0.05; **p < 0.01; ****p < 0.0001.